Review Article

Nano Research
2020, 13(1): 18–37

ISSN 1998-0124 CN 11-5974/O4
https://doi.org/10.1007/s12274-019-2589-z

Graphitic carbon nitride with different dimensionalities for energy and environmental applications

Qiang Hao[1], Guohua Jia[2], Wei Wei[1], Ajayan Vinu[3], Yuan Wang[4], Hamidreza Arandiyan[5], and Bing-Jie Ni[1] (✉)

[1] *Centre for Technology in Water and Wastewater (CTWW), School of Civil and Environmental Engineering, University of Technology Sydney (UTS), Sydney, NSW 2007, Australia*
[2] *Curtin Institute of Functional Molecules and Interfaces, School of Molecular and Life Sciences, Curtin University, Perth, WA 6845, Australia*
[3] *Global Innovative Centre for Advanced Nanomaterials (GICAN), School of Engineering, Faculty of Engineering and Built Environment, The University of Newcastle, Callaghan, NSW 2308, Australia*
[4] *School of Chemistry, Faculty of Science, The University of New South Wales, Sydney, NSW 2052, Australia*
[5] *Laboratory of Advanced Catalysis for Sustainability, School of Chemistry, The University of Sydney, Sydney, NSW 2006, Australia*

Received: 9 October 2019 / **Revised:** 20 November 2019 / **Accepted:** 28 November 2019

ABSTRACT

As a metal-free semiconductor, graphitic carbon nitride (g-C_3N_4) has received extensive attention due to its high stability, nontoxicity, facile and low-cost synthesis, appropriate band gap in the visible spectral range and wide availability of resources. The dimensions of g-C_3N_4 can influence the regime of the confinement of electrons, and consequently, g-C_3N_4 with various dimensionalities shows different properties, making them available for many stimulating applications. Although there are some reviews focusing on the synthesis strategy and applications of g-C_3N_4, there is still a lack of comprehensive review that systemically summarises the synthesis and application of different dimensions of g-C_3N_4, which can provide an important theoretical and practical basis for the development of g-C_3N_4 with different dimensionalities and maximises their potential in diverse applications. By reviewing the latest progress of g-C_3N_4 studies, we aim to summarise the preparation of g-C_3N_4 with different dimensionalities using various structural engineering strategies, discuss the fundamental bottlenecks of currently existing methods and their solution strategies, and explore their applications in energy and environmental applications. Furthermore, it also puts forward the views on the future research direction of these unique materials.

KEYWORDS

graphitic carbon nitride, micro-nano structure, energy functional materials, environmental functional materials, photocatalyst

1 Instructions for using the template

According to the dimensionality of the nanostructure and their components, materials can be classified into zero-dimensional (0D), one-dimensional (1D), two-dimensional (2D) and three-dimensional (3D) materials [1, 2]. 0D materials are nanosized particles whose width and length are in the nanometre range, in which electrons are confined in three dimensions. Quantum dots, nanoparticles and nanopowders are the few examples of 0D materials [3–5]. Materials are considered as 1D materials in which one dimension is outside the nanoscale wherein electrons have confinement in two directions and nanowires, nanotube and nanorod are all typical 1D materials [6–12]. The 2D materials refer to the materials in which electrons are confined at a non-nanoscale, such as nanofilm, nanosheet, superlattice and quantum well [13–26]. The 3D nano-materials preserve some superiorities of nano-size effect, but electrons in 3D materials can move freely in three non-nanoscale scales [12, 27, 28]. Due to the confinement of the nanostructure to electrons, materials with different dimensionality have highly profoundly different performance in various fields. Nanostructured materials with different dimensions exhibit unique structural features, and elemental composition has unique semiconducting, conducting and insulating properties in various fields. Among these nanostructures, carbon nitride-based nanomaterials have received a lot of attention owing to their unique semiconducting and essential properties and high thermal and chemical stability [29–32]. Based on the dimensionality and the chemical structure and composition, the properties of these unique materials are varied.

The study of carbon nitride (CN) can be dated back to 1834 when Berzelius firstly obtained a linear CN polymer and named it as "melon" [33, 34]. Since then, the investigation of CN has begun. In 1922, Franklin discovered a type of graphitic carbon nitride (g-C_3N_4) by the thermal decomposition of mercuric thiocyanate [35]. In 1989, it was predicted that if C could replace Si in the structure of β-Si_3N_4, a super hard β-C_3N_4 material could be obtained [36]. In 1996, Teter and Hemley predicted five types of CN with different phases including α-C_3N_4, β-C_3N_4, c-C_3N_4, p-C_3N_4 and g-C_3N_4 (Fig. 1) [37]. According to the crystal structure, the CNs are all super hard materials except for g-C_3N_4 [38]. Thus, it is much easier to modify the morphology and structures of g-C_3N_4. As a result, the study of g-C_3N_4 became a hot topic, and a series of g-C_3N_4 with different structures and functionalities have been reported.

Address correspondence to bingjieni@gmail.com

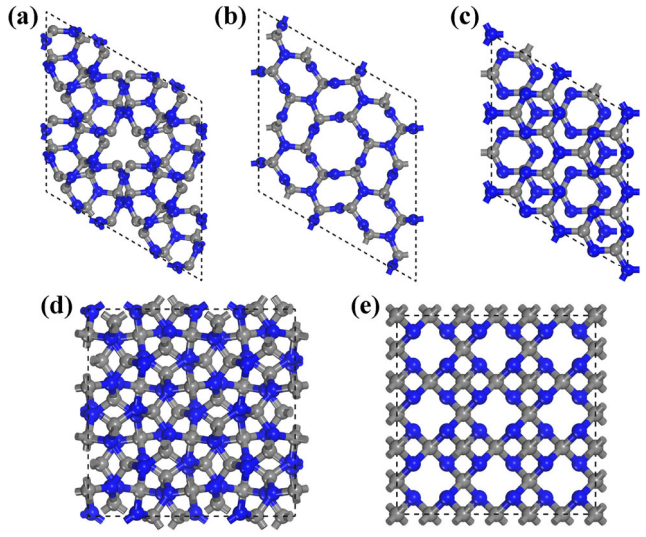

Figure 1 Structure of (a) α-C_3N_4, (b) β-C_3N_4, (c) g-C_3N_4, (d) cubic-C_3N_4 and (e) pseudocubic-C_3N_4 view from the [001] axis. The grey spheres represent carbon atoms, and the blue spheres represent nitrogen.

In g-C_3N_4, both C and N atoms are sp^2 hybridised. They are connected by σ bonds, forming a hexagonal structure. This hexatomic ring is called triazine ring. Each of the triazine rings is linked to a small unit, which is connected by a C–N bond. It is generally accepted that graphitic carbon nitride may have two chemical structures: g-C_3N_4 with a triazine ring (C_3N_3) which belongs to an *R*3*m* space group and other one has the structure that consists of a tri-s-triazine ring (C_6N_7) with a space group of *P*6*m*2 [39]. In g-C_3N_4, each triazine ring is connected by the N atom at the end, forming an infinitely expanded planar grid structure. From the illustrational graph of g-C_3N_4 (Fig. 2(a)), the length of C–N bond in the g-C_3N_4 ring is 0.1315 nm and the C–N–C bond angle is 116.5 °C. The length of C–N bond outside the g-C_3N_4 ring is 0.1444 nm and the C–N–C bond angle is also 116.5 °C. In Fig. 2(b), the length of C–N bond in the g-C_3N_4 ring is 0.1316 nm and the C–N–C bond angle is 116.6 °C. The length of C–N bond outside the g-C_3N_4 ring is 0.1442 nm and the C–N–C bond angle is also 120.0 °C [39]. In these two allotropes, the electronic structure and thermodynamic stability are different because of the different-sized nitrogen holes in the structure. It is reported that the g-C_3N_4 with the tri-s-triazine ring is more thermodynamically stable than that with triazine structure [40].

In these two types of g-C_3N_4, both C and N atoms belong to sp^2 hybridisation, which can form highly conjugated π bonds with the lone electron pairs on p_z orbitals. As a result, a highly delocalized conjugated system is composed. The absorption edge of g-C_3N_4 is about 460 nm and its bandgap is about 2.7 eV, with the conduction band (CB) at −1.13 eV and the valence band (VB) at +1.74 eV [41–43]. Since the low-coordinated N atoms contribute to both the CB and VB, the significant π bonds formed have low delocalisation, which is one of the main reasons for the relatively high electron–hole recombination rate of bulk g-C_3N_4. Generally, thermal decomposition of high nitrogen-containing carbon precursors is one of the most commonly used techniques for the synthesis of g-C_3N_4. However, the obtained g-C_3N_4 is usually bulk and non-porous in nature with a strong van der Waals forces between g-C_3N_4 layers. As a result, the bulk g-C_3N_4 exhibits poor specific surface area with irregular stacking of thick layers, which significantly restricts its application in catalysis due to the limited contact area with reactants. In addition, the photogenerated charge carriers cannot rapidly transfer to the surface of materials to participate in the reaction, which greatly reduces the separation and transfer efficiency of photogenerated carriers and limits the catalytic performance of g-C_3N_4. More importantly, the calcined g-C_3N_4 has a low polymerisation degree, low crystallinity and abundant surface defects, which deteriorate its performances and impede its widespread applications in various fields covering sensing, adsorption and separation and catalysis. The dimension of g-C_3N_4 is another important factor that can be controlled by altering the synthesis parameter. The control of dimensions plays a significant role in the performance of these nanostructures towards various applications related to the energy and environment, as the influence on the specific surface area, pore structure, optical properties, transfer path, and separating rate of electron–hole pairs of the g-C_3N_4.

The schematic illustration of the transitions among bulk, 0D, 1D, 2D g-C_3N_4 and 3D g-C_3N_4 is shown in Fig. 3. Like graphene, g-C_3N_4 manifests 2D layered structure. In each layer, the 3-s-triazine rings are bound by forming an infinitely expanded network-like planar structure, while interlayer interaction is van der Waals forces. Therefore, inspired by graphene stripping, 2D g-C_3N_4 nanosheets with the larger specific surface area can also be obtained by stripping bulk g-C_3N_4. Besides, 0D and 1D g-C_3N_4 can be synthesised by modifying the number and arrangement of structural units. For example, template growth method can be used to synthesise 1D g-C_3N_4. Via different methods, 0D, 1D, 2D and bulk g-C_3N_4 can be prepared. Under the treatment of solution and external force, bulk g-C_3N_4 can be converted into 0D, 1D, 2D or 3D structure. In the meanwhile, 0D g-C_3N_4 can also be assembled into 1D g-C_3N_4, and 2D g-C_3N_4 can be converted into 1D nanostructure with special treatment. Thus, it is significant to develop g-C_3N_4 with various dimensionality to maximise its potential in diverse applications.

Currently, most researchers pay attention to the modification strategies of g-C_3N_4 to improve its photocatalytic performance

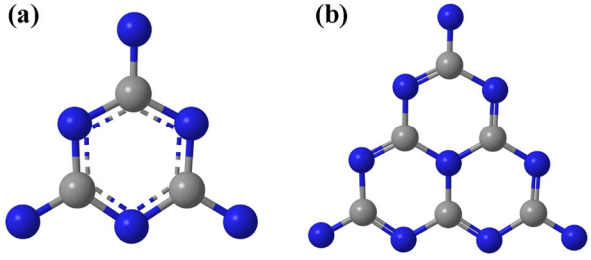

Figure 2 Triazine- (a) and tri-s-triazine-based connection patterns (b) of potential g-C_3N_4 allotropes.

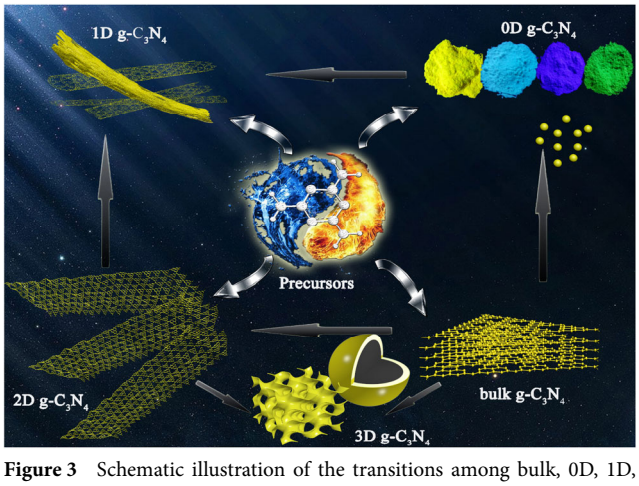

Figure 3 Schematic illustration of the transitions among bulk, 0D, 1D, 2D and 3D g-C_3N_4.

[44–48], including energy conversion, pollutant degradation [49–51], and microbial control etc. [52]. Although there are a few reviews focusing on the strategies for the modification of g-C_3N_4, such as the construction of g-C_3N_4-based heterostructure photocatalysts or elements doping [53, 54], as well as the first-principle calculation studies on tri-s-triazine-based g-C_3N_4 or magnetically separable g-C_3N_4 [55, 56], a comprehensive review on the synthesis of g-C_3N_4 with various dimensionalities and their effects on various applications related to energy and environment is still lacking. In this work, we provide an up-to-date review of the synthetic methods of g-C_3N_4 with various dimensionalities and its energy and environmental-related applications. We also give a brief overview of the research status and propose the future development trend of g-C_3N_4 and their potential applications.

2 General synthesis of g-C_3N_4

Various synthetic approaches have been developed for the preparation of a variety of low-dimensional g-C_3N_4 through a simple treatment of bulk g-C_3N_4. In this section, we firstly summarise various synthetic approaches of bulk g-C_3N_4, which mainly include solid-state reaction, electrochemical deposition, solvothermal reaction and thermal decomposition (Fig. 4).

2.1 Solid-state reaction

The solid-state reaction is generated by contact, reaction, nucleation, and crystal growth between solid interfaces at high temperature [57–59]. This was successfully applied by Kouvetakis et al. in 1994, who reported on the preparation of 2,4-difluoro-6-bis(trimethylsilyl)imido-l,3,5-triazine and 2,4-dichloro-6-bis(trimethylsilyl)imido-1,3,5-triazine and used them as precursors to fabricate thin films of C_3N_4 [60]. Khabashesku et al. also synthesised g-C_3N_4 via the reaction of lithium nitride with cyanuric chloride or its fluoro analogue in a stainless steel reactor [61]. Reaction parameters such as synthesis temperature and pressures are varied to control the morphology, crystallinity and the dimensionalities and the properties of the g-C_3N_4. For example, Zhang et al. reported two strategies for the synthesis of g-C_3N_4, one of which is the self-reaction of 2-amino-4,6-dichloro-1,3,5-triazine and the other is the reaction of melamine and cyanuric chloride. Both approaches were carried out at the pressures between 1.0 and 1.5 GPa and the temperatures of 500 to 600 °C [62]. Gu et al. prepared g-C_3N_4 using calcium cyanamide and cyanuric chloride as a reactant precursor at about 550 °C [63]. However, the prepared sample was contaminated with calcium chloride and required an additional purification process to obtain a high-quality g-C_3N_4. In 2007, Lu et al. adopted a high-pressure approach to preparing g-C_3N_4 material with tunable crystallinity [64]. In this approach, 1,3,5-trichlorotriazine and sodium azide were mixed for the reaction under 40 MPa and 220 °C. It is worth noting that the crystallinity of g-C_3N_4 was increased as the pressure of the vessel was increased. Most importantly, the morphology was also changed into nanowires when Zn particles were added into the reactor.

2.2 Electrochemical deposition

Electrochemical deposition is a technique in which current migrates through positive and negative ions in an electrolyte solution under the influence of an external electric field, and electrons are oxidised and reduced on the electrodes to form coatings. This technique has been quite attractive as it can improve the quality and properties of products [65–67]. Fu et al. first used electrodeposition technique for the preparation of g-C_3N_4 from the solution of dicyandiamide in acetone [68]. Various precursors in different solvents have been employed in this technique for controlling the properties of g-C_3N_4. Li et al. successfully demonstrated the room temperature fabrication of highly crystalline g-C_3N_4 thin films with the acetonitrile solution of melamine and cyanuric chloride through a simple electrochemical deposition [69]. Templating approach, coupled

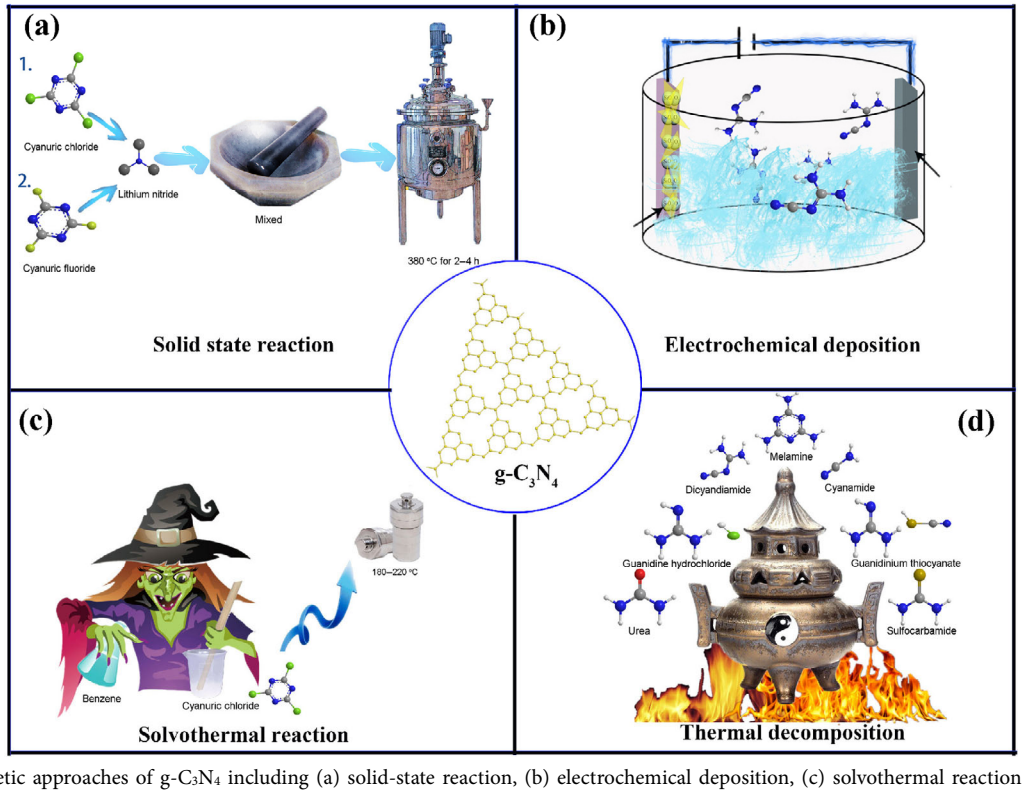

Figure 4 Synthetic approaches of g-C_3N_4 including (a) solid-state reaction, (b) electrochemical deposition, (c) solvothermal reaction and (d) thermal decomposition.

with the electrochemical deposition, was used for the control of morphology and the particle diameter of g-C_3N_4. For example, Bai et al. reported hollow g-C_3N_4 microspheres using silica nanospheres with different diameters as templates. The average diameters of the spheres are about 1 μm, and they are composed of nanoparticles with a size range of 5 to 30 nm [70].

2.3 Solvothermal reaction

Solvothermal is a synthetic method of reacting the original mixture in an airtight system (such as an autoclave) with organic or non-aqueous solvents at certain temperature and pressure in the solution. The materials obtained by this method have good crystallinity, controllable morphology and good dispersity [71–74]. In 2000, Montigaud et al. reported the first synthesis of g-C_3N_4 by a solvothermal reaction with melamine and cyanuric chloride in triethylamine under 130 MPa and 250 °C [75]. Guo et al. used cyanuric chloride and sodium amide via benzene-thermal reaction at 180–220 °C to prepare g-C_3N_4 nanocrystallites [76]. Interestingly, when sodium amide was replaced with sodium azide, g-C_3N_4 nanotubes were obtained, probably because sodium azide might affect crystal growth, and alignment [77]. Bai et al. prepared g-C_3N_4 by heating carbon tetrachloride and ammonium chloride at 400 °C [78]. Additionally, solvothermal reaction of dicyandiamide or melamine in carbon tetrachloride at 290 °C and 4.5 MPa can also produce g-C_3N_4 [79].

2.4 Thermal decomposition

Thermal decomposition is one of the most commonly used synthetic approaches for mass production of g-C_3N_4, due to its wide resources, facile operation and low cost. In 2000, Gillan reported a synthesis of g-C_3N_4 via the thermal decomposition of 2,4,6-triazido-1,3,5-triazine [80]. The obtained samples had different C/N ratios when the reaction was conducted at different reaction temperatures and pressures. Lotsch and Schnick used ammonium, guanidinium and melaminium to modify tricyanomelaminate to obtain CN_x [81]. They proposed the possible decomposition pathways as fallow: Upon heating, ammonium and guanidinium tricyanomelaminate uniformly passed through the crystalline, heptazine (C_6N_7)-based intermediate melem ($C_6N_7(NH_2)_3$), which decomposed and formed a semi-amorphous CN_xH_y material with a pronounced layered structure. Identical pyrolysis products were obtained for the melaminium salt, a classical triazine (C_3N_3)-based CN_x precursor, after passing an intermediate, possibly cross-linked phase at low temperatures. The thermal decomposition of nitrogen-rich precursors such as cyanamide, dicyandiamide, melamine, urea, sulfocarbamide, guanidinium thiocyanate or guanidine hydrochloride can also be used to prepare g-C_3N_4 [82–89].

Overall, solid-state reaction, electrochemical deposition, solvothermal reaction and thermal decomposition can all be used to prepare g-C_3N_4. The solid-state reaction requires high temperature and high pressure, which is high-cost and environmentally unfriendly, thus it is not applied widely. With electrochemical deposition, g-C_3N_4 film or spheres can be obtained at room temperature, which may have more wide application, such as sensor or photoelectrocatalyst. While this approach may be not suitable for mass production. The solvothermal reaction can also be used to prepare g-C_3N_4 with special morphology, while this process is more complex, and it needs high pressure. Using thermal decomposition method to synthesize g-C_3N_4 is the most widely applied approach, as it has facile operation and low cost. However, the process needs a lot of heat and a large amount of ammonia will be generated. What is worse, the g-C_3N_4 obtained by the thermal decomposition method usually has a bulk structure, which limits its performance in various area. All in all, different syntheses of g-C_3N_4 have different advantages and researchers should consider what they want when they want to select a proper approach to preparing g-C_3N_4.

3 Synthesis of various dimensions of g-C_3N_4

3.1 0D g-C_3N_4

0D g-C_3N_4 is also termed as g-C_3N_4 quantum dots (CNQDs), in which electrons and holes are unable to move freely. Many synthetic methods of CNQDs have been reported, such as microwave-assisted synthesis, solid state reaction and exfoliation of bulk g-C_3N_4. In 2011, Liu et al. prepared CNQDs with excellent photoluminescent (PL) with CCl_4 and 1,2-ethylenediamine (EDA) by separate methods, including facile refluxing, microwave, or solvothermal heating [90]. Besides, they also developed an acid-driven and microwave-assisted approach to synthesise CNQDs using N,N-dimethylformamide (DMF) as the solvent [91]. The microwave heating of organic amines (dimethylamine (DIA), ethylamine (EA) or tripropylamine (TPA)) and acid can also be employed to fabricate CNQDs [92]. In 2012, Barman and Sadhukhan employed a facile microwave mediated synthesis of highly blue fluorescent CNQDs using formamide as a precursor [93]. The prepared CNQDs has high efficiency as sensors to detect mercuric and iodide ions in aqueous. Tang et al. used guanidine hydrochloride and EDTA as precursors to prepare CNQDs by a microwave-assisted approach [94]. The obtained chemiluminescence CNQDs was used to detect free residual chlorine in water (Figs. 5(a) and 5(b)). Li et al. used microwave oven (700 W) to heat the mixture of citric acid, thiourea and water to produce CNQDs [95]. Microwave heating of the mixture of citric acid monohydrate, urea and oleic acid are also reported as an approach for the synthesis of CNQDs [96]. Besides the microwave-assisted method, solid-state reaction can also be used to prepare CNQDs. Zhou et al. reported a facile synthesis of CNQDs with highly florescent and tunable emission by heating the mixture of urea and sodium citrate of different ratios at 180 °C [43]. In addition to synthesising CNQDs with small nitrogen-containing organic molecules, exfoliating bulk g-C_3N_4 is also an important strategy to prepare CNQDs. In 2014, Zhang et al. reported a way to tailor bulk g-C_3N_4 [97]. Firstly, bulk g-C_3N_4 was treated by a mixture of sulfuric acid (H_2SO_4) and nitric acid (HNO_3). After that, the produced porous g-C_3N_4 was dispersed in ammonia monohydrate ($NH_3{\cdot}H_2O$) and heated at 180 °C for 12 h. During this progress, porous g-C_3N_4 transferred to porous nanosheets. Then the porous g-C_3N_4 nanosheets were dispersed in water and sonicated for 6 h. After being dialyzed, CNQDs was successfully achieved, which can be used for imaging of cellular nucleus by two-photon fluorescence (Fig. 5(d)). Although this method can be used to fabricate CNQDs, it is too complex as it involves many steps. To simplify the exfoliating process, Bai et al. developed a more facile synthesis to tailor bulk g-C_3N_4 by stirring, sonicating and heating bulk g-C_3N_4 in the mixture of H_2O_2 and $NH_3{\cdot}H_2O$. The obtained CNQDs have much better photocatalytic activity in hydrogen production than bulk g-C_3N_4 [98].

CNQDs can also be prepared by sonicating bulk g-C_3N_4 in acid (mixture of H_2SO_4 and HNO_3) and filtered with microporous membrane [99]. Wang et al. used a modified Hummers method to prepare CNQDs by tailoring bulk g-C_3N_4 with concentrated H_2SO_4, $NaNO_3$, H_2O_2 and potassium permanganate ($KMnO_4$) [100]. Song et al. used HNO_3 to treat bulk g-C_3N_4 and heated the suspension at 200 °C for 12 h to obtain CNQDs [101]. Acid tailor can be used to synthesise CNQDs, but it is not

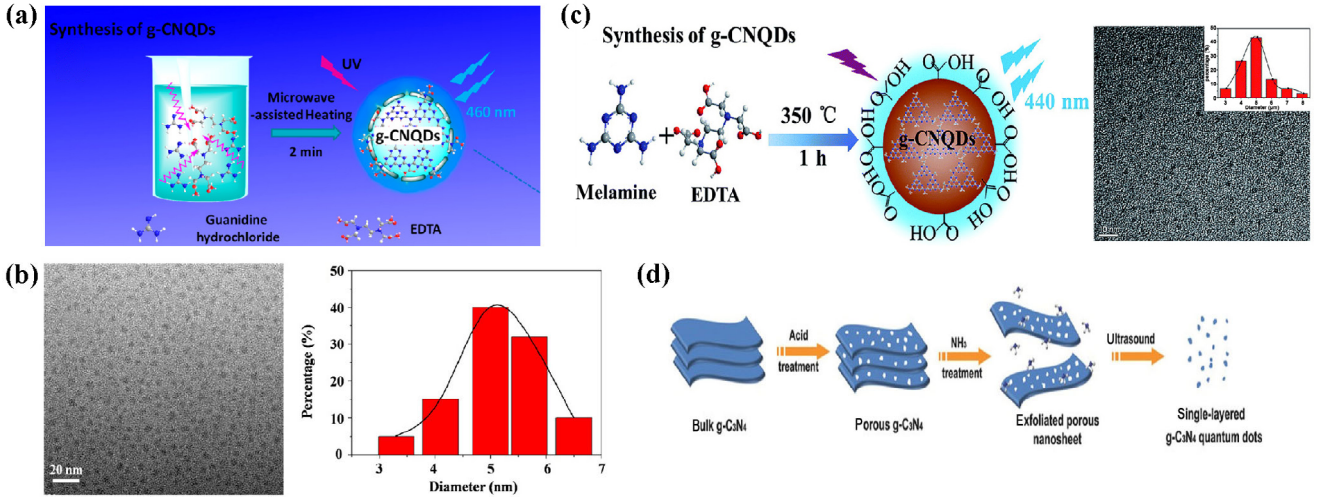

Figure 5 (a) Schematic illustration for the preparation of CNQDs by a microwave-assisted method; (b) the TEM image and size distribution of the prepared CNQDs (reproduced from Ref. [94] with permission, © American Chemical Society 2014). (c) Schematic illustration for preparation of CNQDs through a thermal condensation process, TEM image of obtained prepared CNQDs and its size distributions (reproduced from Ref. [102] with permission, © The Royal Society of Chemistry 2015). (d) Schematic illustration of the strategy for the preparation of CNQDs (reproduced from Ref. [97] with permission, © Wiley-VCH 2014).

environmentally friendly as this method consumes a large amount of acid. Fan et al. reported a facile and green tailor method to prepare CNQDs. Firstly, the uniform mixture of melamine and ethylenediamine tetra acetic acid (EDTA) was heated at 350 °C of 1 h. Then the products were dissolved in water and purified by dialysis membrane. CNQDs obtained by this method can be used in chemiluminescent dopamine sensing (Fig. 5(c)) [102].

3.2 1D g-C_3N_4

In 1D g-C_3N_4, electrons can only move freely in one direction. g-C_3N_4 with such characteristics usually refers to g-C_3N_4 micro-nano rods, g-C_3N_4 micro-nano tubes and g-C_3N_4 micro-nano wires. Herein, the synthetic approaches of 1D g-C_3N_4 and its relevant applications are discussed in detail.

3.2.1 g-C_3N_4 micro-nano rods

Template-assisted methods have been employed for the synthesis of g-C_3N_4 micro-nano rods. In 2011, Li et al. prepared g-C_3N_4 micro-nano rods using anodic alumni oxide (AAO) membrane as a template (Fig. 6(a)) [103]. This method provides an efficient way to improve the crystallinity of g-C_3N_4 and water splitting ability, for the better optical absorption and charge-carriers separation. Other templates such as SBA-15 silica or SiO_2 micro-nano rods can also be employed to fabricate g-C_3N_4 micro-nano rods with excellent photocatalytic activity for hydrogen evolution reactions [104, 105]. Template-assisted method is easy to operate, while strong acid or alkali is needed to remove the templates. Heating bulk g-C_3N_4 in solutions can also obtain g-C_3N_4 micro-nano rods. Bai et al. stirred and refluxed bulk g-C_3N_4 in methanol-water solution, and they got high performance g-C_3N_4 micro-nano rods on the degradation of organic pollutants in water (Fig. 6(b)) [106]. Firstly, bulk g-C_3N_4 transfer to nanosheets in methanol. During the process of reflux, some surface defects of g-C_3N_4 nanosheets are repaired, which may result in the rolling of nanosheets on edge, producing g-C_3N_4 micro-nano rods. Xu et al. used a more facile solvothermal method (NH_4Cl solution) to modify bulk g-C_3N_4, and they also obtained g-C_3N_4 micro-nano rods with photoelectrochemical sensing of trace Cu^{2+} ions [107]. Hu et al. calcined the mixture of thiourea and ammonium hydrogen phosphate to prepare S and P co-doped g-C_3N_4. Then the S and P co-doped g-C_3N_4 was transferred to a 100 mL Teflon inner liner with 80 mL water in it and heated to 150 °C. After the hydrothermal reaction, the obtained S and P co-doped g-C_3N_4 turned out to be micro-nano rods and had much better performance on degrading organic pollutants [108]. Tang et al. used H_2SO_4, HNO_3 and hydrogen chloride (HCl) to treat melamine, and they obtained g-C_3N_4 micro-nano rods with various lengths, diameters and specific surface area (A_{BET}) [109]. All the g-C_3N_4 micro-nano rods have higher photocatalytic activity than bulk g-C_3N_4. Can g-C_3N_4 be synthesised by direct thermal decomposition reaction? Li et al. reported a very interesting synthesis of g-C_3N_4 micro-nano rods [110]. In a typical synthesis, a certain amount of dicyandiamide was spread on the bottom of an alumina boat, and another empty alumina boat was covered on top of it. Then they used infrared (IR) light to heat the precursors to achieve g-C_3N_4 micro-nano rods. The formation of micro-nano rods structure was attributed to the unique IR heating, and the obtained samples showed excellent photocatalytic water splitting ability.

3.2.2 g-C_3N_4 micro-nano tubes

Chemical vapour deposition (CVD) is an effective approach for preparing well-constructed C_3N_4 micro-nano tubes, although it requires complex and expensive equipment [111, 112]. Tragl et al. prepared several types of g-C_3N_4 micro-nano tubes with cyanuric chloride and various nitrogen sources. In this synthesis, $N(C_3N_3Cl_2)_3$ formed initially in the reaction process can act as the template for the formation of micro-nano tube structure [113]. Bian et al. used AAO membrane as the template to prepare g-C_3N_4 micro-nano tubes [114]. The obtained g-C_3N_4 micro-nano tubes were used as the support of platinum particles constituting hybrid Pt-g-C_3N_4 micro-nano tubes, which can be used as catalyst carriers in cyclohexene hydrogenation. Except for CVD and template methods, some special treatment can also be used to obtain g-C_3N_4 micro-nano tubes. Li et al. mixed cyanuric chloride and melamine with ball crusher and heated the precursors at 150 °C for 24 h to remove moisture and oxygen [115]. Moreover, then the solid was calcined at 800 °C in vacuum electric furnace to obtain g-C_3N_4 tubes. Cao et al. heated cyanuric chloride and sodium with Ni-based catalyst in a stainless steel autoclave to prepare g-C_3N_4 micro-nano tubes [116]. Cyanuric acid, melamine and caffeine can form a

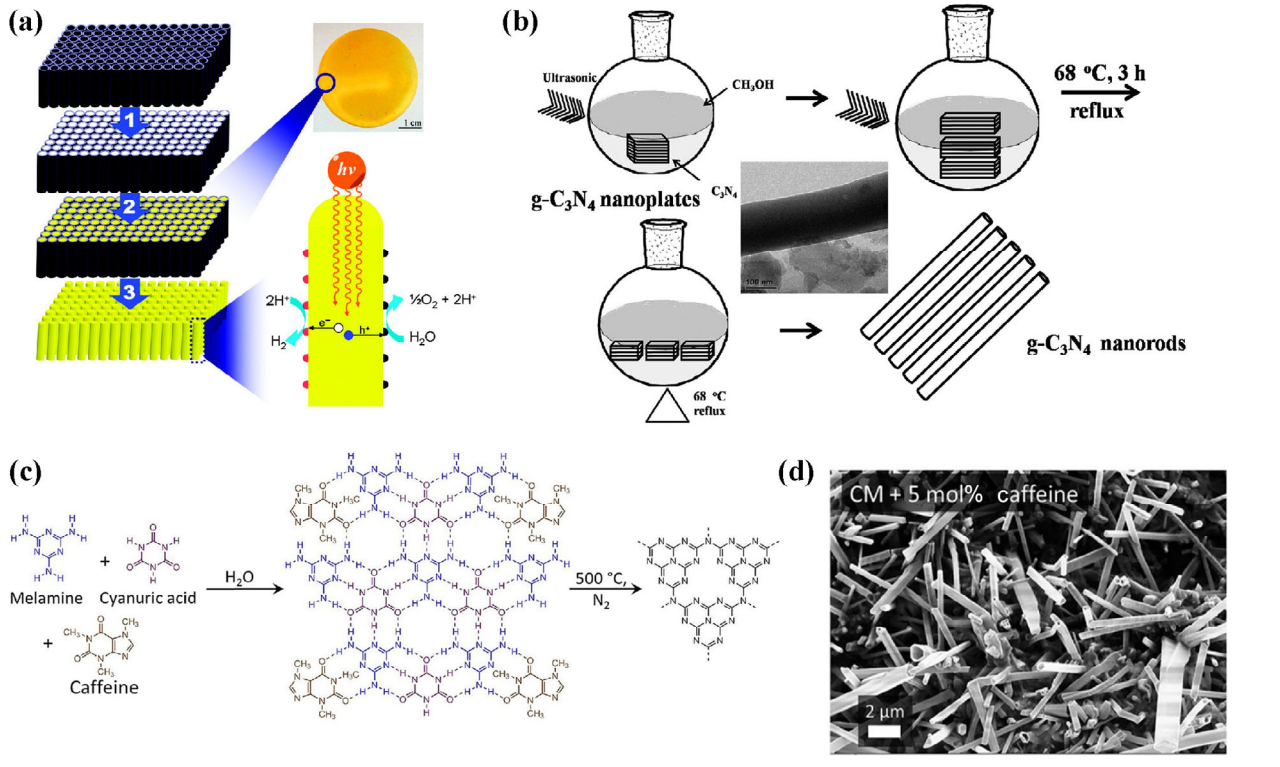

Figure 6 (a) Schematic illustration for the preparation of g-C_3N_4 nanorods (reproduced from Ref. [103] with permission, © American Chemical Society 2011). (b) Schematic illustration of the formation process of g-C_3N_4 nanorods from g-C_3N_4 nanoplates and its TEM image (reproduced from Ref. [106] with permission, © American Chemical Society 2013). (c) Reaction path of caffeine-modified g-C_3N_4 nanotubes from cyanuric acid-melamine supramolecular complexes and (d) its SEM image (reproduced from Ref. [117] with permission, © Wiley-VCH 2015).

supramolecular complex, which formed g-C_3N_4 micro-nano tubes after calcination (Figs. 6(c) and 6(d)). The g-C_3N_4 micro-nano tubes have better photocatalytic performance than bulk g-C_3N_4 [117]. Guo et al. prepared phosphorous-doped g-C_3N_4 micro-nano tubes by the treatment of precursor [118]. Firstly, melamine and phosphorous acid were dissolved in deionised water and heated in a Teflon liner at 180 °C for 10 h. Then the samples were washed, dried and calcined, resulting in the formation of phosphorus-doped g-C_3N_4 micro-nano tubes. The hydrothermal reaction product was washed several times to completely remove the phosphorous acid, the final product obtained was g-C_3N_4 micro-nano tubes (Figs. 7(a) and 7(b)). By hydrothermal treatment heating procedure at 500 °C for 4 h, Jin et al. also successfully prepared g-C_3N_4 micro-nano tubes [119].

3.2.3 *g-C_3N_4 micro-nano wires*

g-C_3N_4 micro-nano wires is also a type of 1D g-C_3N_4 materials which have multi functionalities. In 2013, Tahir used a template-free method to prepare g-C_3N_4 micro-nano wires [120]. Firstly, melamine was dissolved in ethanol and treated by HNO_3. Then the product was washed, dried and heated to 450 °C in a CVD furnace to produce g-C_3N_4 micro-nano wires (Figs. 7(c) and 7(d)). The synthesised g-C_3N_4 micro-nano wires have better optical, electrochemical and photocatalytic performance than bulk g-C_3N_4. Cyanuric chloride-melamine complex was also used as the precursor to fabricate g-C_3N_4 micro-nano wires using a 100 mL Teflon-lined autoclave. g-C_3N_4 micro-nano wires can be obtained after the calcination of the obtained powder at 500 °C. The g-C_3N_4 micro-nano wires obtained using this approach have better photocatalytic degradation efficiency than bulk g-C_3N_4 [121]. Han et al. prepared g-C_3N_4 micro-nano wires by another method [122]. The used ultrasonic to make dicyandiamide dissolved in water. After that, the precursor was put in a Teflon-lined autoclave and kept at 200 °C for 4 h. Then it was frozen in liquid nitrogen to freezing assisted assembly. Finally, the powder was heated to 500–650 °C and g-C_3N_4 micro-nano wires with better photocatalytic hydrogen evolution ability were obtained. Zhang et al. reported a method of tailoring iodine-doped bulk g-C_3N_4 to quantum dots and its self-assembly to synthesis g-C_3N_4 micro-nano wires [123]. Firstly, they prepared the iodine-doped bulk g-C_3N_4. Then hydrothermal reaction in H_2O_2 solution was employed to downsize the bulk-iodine-doped g-C_3N_4. As a result, g-C_3N_4 quantum dots can be obtained, which gradually self-assembled to g-C_3N_4 micro-nano wires in solvents with different polarities. By changing the solvents, the g-C_3N_4 micro-nano wires with different diameters, tunable bandgaps can be obtained.

In summary, the synthesis methods of 1D g-C_3N_4 including g-C_3N_4 micro-nano rods, g-C_3N_4 micro-nano tubes and g-C_3N_4 micro-nano wires were summarised. The electrons in 1D g-C_3N_4 have free movement in the elongated direction of the particles, resulting in a significantly promoted separation efficiency of photogenerated charge carriers, which illustrates the reason why 1D g-C_3N_4 is mostly applied as photocatalysts. Due to its low luminescence quantum efficiency, 1D g-C_3N_4 is not suitable for the applications in lighting and displays. Template method is one of the most frequently used approaches to achieve 1D g-C_3N_4. As the examples mentioned above, g-C_3N_4 micro-nano rod arrays and g-C_3N_4 micro-nano tube arrays can be prepared by using AAO as templates. Employing physical (thermal, ultrasonic, high-pressure and mechanical effect) and chemical effects can exfoliate and re-assemble bulk g-C_3N_4 into 1D structure. Besides, physical and chemical treatment may influence the phase, crystallinity and arrangement of the precursors, and result in the formation of 1D g-C_3N_4 with distinguished properties.

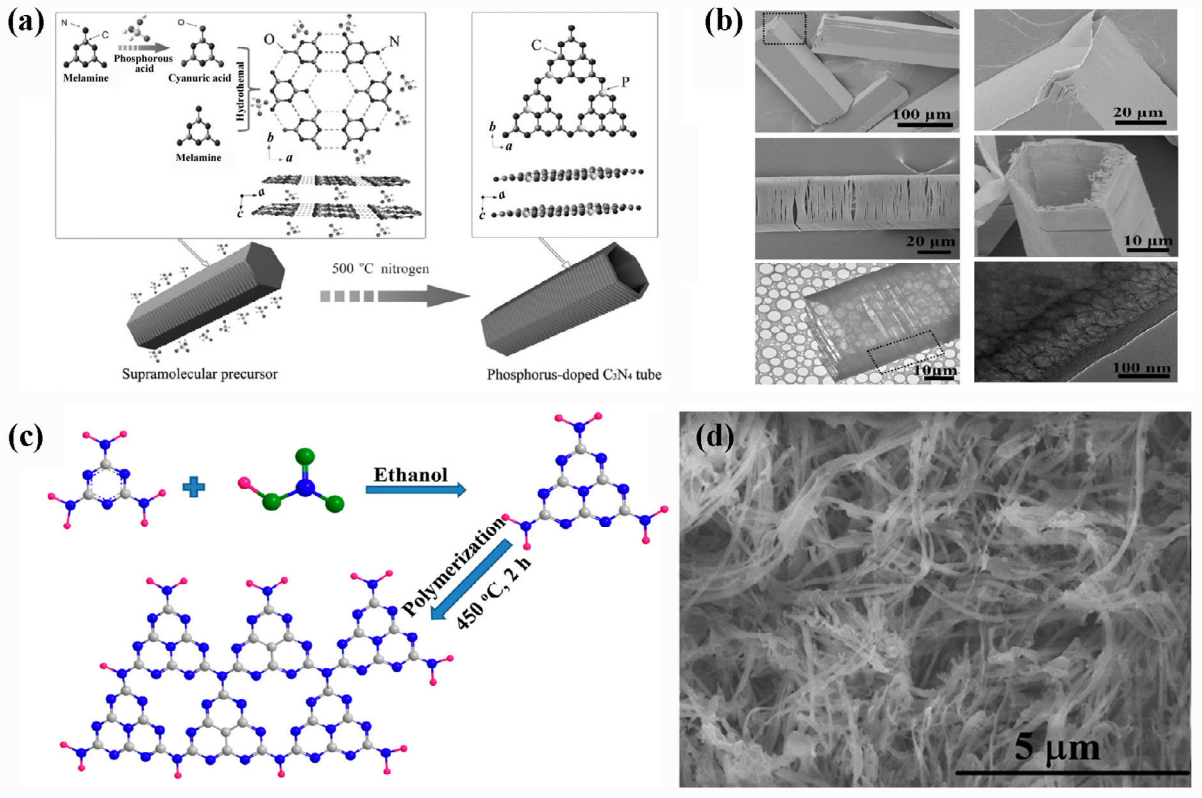

Figure 7 (a) The formation process of phosphorus-doped g-C_3N_4 nanotubes; (b) the SEM and TEM images of prepared g-C_3N_4 nanotubes (reproduced from Ref. [118] with permission, © Wiley-VCH 2016). (c) Schematic representation of chemical reaction for the synthesis of g-C_3N_4 nanowires and (d) its SEM image (reproduced from Ref. [120] with permission, © American Chemical Society 2014).

3.3 2D g-C_3N_4

2D g-C_3N_4 usually refers to g-C_3N_4 nanosheets in which electrons are predominantly confined in the thickness direction and can only move freely in two dimensions. As a result of this, we summarised the synthetic methods of 2D g-C_3N_4.

3.3.1 Post-calcined method

The post-calcined method is a facile top-down strategy to weaken the van der Waals forces between bulk g-C_3N_4 layers for the synthesis of g-C_3N_4 nanosheets [124]. Niu et al. calcined bulk g-C_3N_4 at 500 °C for 2 h and obtained g-C_3N_4 nanosheets with a thickness of around 2 nm [124]. The nanosized g-C_3N_4 has a much larger specific surface area, enhanced transfer of electrons along an in-plane direction, longer lifetime of charge carriers and enhanced photocatalytic activity (Fig. 8(d)). Li et al. also obtained g-C_3N_4 nanosheets by heating bulk g-C_3N_4 at 520 °C for 4 h and they found that if the heating time is expanded to 6 h, holey ultrathin g-C_3N_4 nanosheets can be obtained [125]. The ultrathin layered and hollow structures led to a highly enhanced photocatalytic hydrogen generation ability (Figs. 8(a)–8(c)). Besides calcination in air, heating bulk g-C_3N_4 in argon gas or ammonia gas can also convert bulk g-C_3N_4 into nanosheets, improving the photocatalytic activity [22, 126].

3.3.2 Liquid exfoliated method

Liquid exfoliated is an approach to prepare low-dimensional materials with the chemical and/or physical effects of solvents and external force (such as ultrasonic wave, pressure or thermal energy). It is another approach to prepare g-C_3N_4 nanosheets. Zhang et al. reported a green liquid exfoliated method to prepare g-C_3N_4 nanosheets (2.5 nm thick) by sonicating bulk g-C_3N_4 in water for 16 h, which showed high performance in bioimaging (Fig. 9) [127]. Due to the strong polarity, water is a better solvent to swell and exfoliate g-C_3N_4 nanosheets compared to ethanol, methanol, DMF or formamide. Sonicating bulk g-C_3N_4 in methanol, isopropanol (IPA), anionic polyacrylamide or anhydrous ethylenediamine can also obtain g-C_3N_4 nanosheets [128–131]. Nevertheless, how can atomic single layer g-C_3N_4 be prepared? In 2013, thin layer of g-C_3N_4 nanosheets (0.4 nm thick) was successfully synthesised by Xu et al., using H_2SO_4 to exfoliate bulk g-C_3N_4 [132]. However, in this preparation method, strong acid (H_2SO_4) is required, which may cause environmental concerns and need extra care in handling. Are there any greener and more facile methods? If post-calcined g-C_3N_4 nanosheets are treated by liquid exfoliated method, the thickness of g-C_3N_4 nanosheets can reduce, and even atomic single layer can be successfully fabricated [133–135].

3.3.3 Other methods

In addition to the methods mentioned above, other methods were also employed to synthesise g-C_3N_4 nanosheets. Bojdys et al. reported an ionothermal method by heating the mixture of dicyandiamide, lithium chloride and potassium chloride to prepare hexagonal g-C_3N_4 nanosheets [136]. Cheng et al. heated melamine and potassium borohydride in argon atmosphere and synthesised g-C_3N_4 nanosheets with a thickness of 1.5 nm [137]. The introduction of potassium borohydride can help weaken the van der Waals force and decrease the planar size of g-C_3N_4 layers. Heating dicyandiamide and ammonium chloride can also obtain g-C_3N_4 nanosheets (Figs. 10(a) amd 10(b)) [138, 139]. Dong et al. prepared g-C_3N_4 nanosheets by calcining the mixture of melamine and cyanuric acids [140]. The product has carbon vacancies and exhibited highly photocatalytic performance in the reduction of NO to N_2 and O_2. Yin et al. reported a liquid ammonia-assisted lithiation method to exfoliate bulk g-C_3N_4 (Figs. 10(c) and 10(d)) [141]. Yu et al. found that using microwave to heat the mixture of

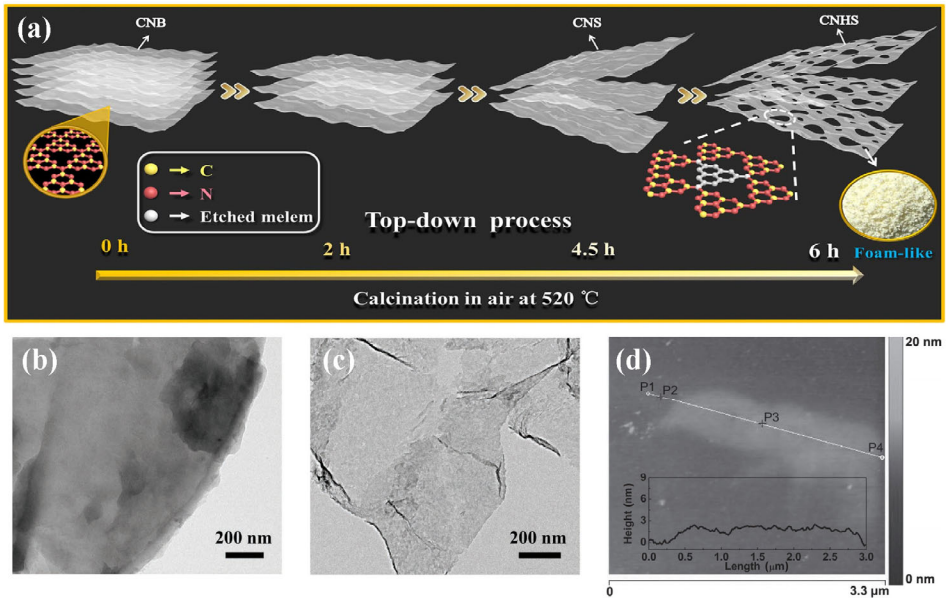

Figure 8 (a) Top-down process for the synthesis of ultrathin g-C_3N_4 nanosheets during post-calcined method. TEM images of bulk g-C_3N_4 (b) and ultrathin g-C_3N_4 nanosheets (c). Reproduced from Ref. [125] with permission, © Wiley-VCH 2016. (d) Tapping-mode AFM image of g-C_3N_4 nanosheets obtained by the post-calcined method (reproduced from Ref. [124] with permission, © Wiley-VCH 2012).

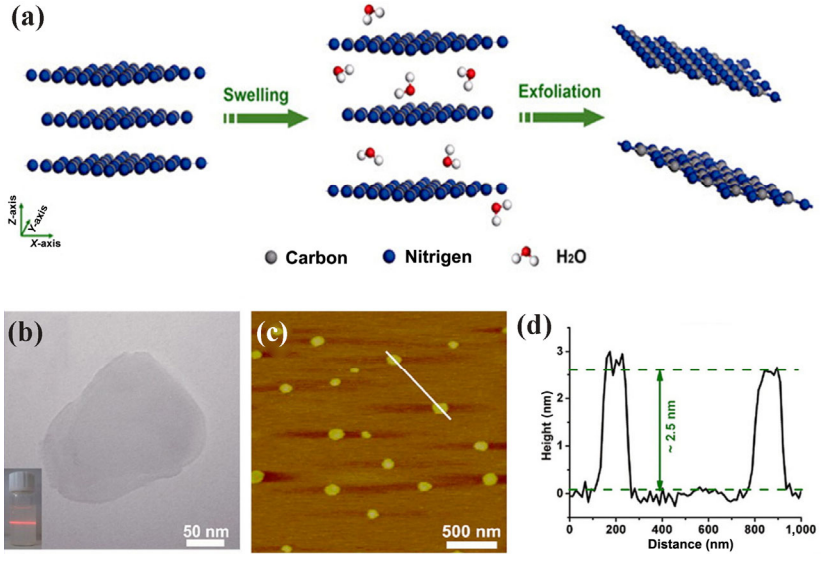

Figure 9 (a) Schematic illustration of liquid-exfoliation process from bulk g-C_3N_4 to ultrathin nanosheets; (b) TEM image and the Tyndall effect of g-C_3N_4 ultrathin nanosheets. (c) AFM image and (d) corresponding height image of the 2D g-C_3N_4. Reproduced from Ref. [127] with permission, © American Chemical Society 2013.

melamine and carbon fibre can produce g-C_3N_4 nanosheets ultra-rapidly [142].

3.4 3D g-C_3N_4

Thermal decomposition is the most commonly used synthetic method for mass production of g-C_3N_4, and it can only be used to produce bulk g-C_3N_4, which is a 3D irregular blocky structure. Some other types of 3D g-C_3N_4 have been developed to overcome the shortages of bulk g-C_3N_4 and broadly functionalise the materials.

3.4.1 Porous 3D g-C_3N_4

Porous materials generally have the advantages of low relative density, high specific strength, high specific surface area and lightweight, and thus can be used in a variety of applications [143]. Dong and Zhang found that replacing melamine with melamine hydrochloride as the precursor, porous 3D g-C_3N_4 can be obtained [144]. The A_{BET} of synthesised porous g-C_3N_4 is 38.8 times as that of bulk g-C_3N_4 and its photocatalytic performance was improved significantly. Liang et al. reported a 3D porous g-C_3N_4 monolith (28 mm × 14 mm × 14 mm) with strong self-support structure [145]. They first made a melamine sponge, completely adsorbed urea, and then heated to 550 °C in N_2 atmosphere. As a result, the 3D porous g-C_3N_4 monolith can be obtained (Fig. 11(a)). Wu et al. prepared a loofa sponge-like 3D network porous N-doped carbon/g-C_3N_4 with excellent oxygen reduction reaction (ORR) and oxygen evolution reaction (OER) performance [146]. Firstly, urea, chitin, NaOH and g-C_3N_4 were dispersed in water. Then the mixture was frozen and thawed several cycles to improve the solubility of chitin. After that, the solution was spread on glass and immersed in ethanol to form a hydrogel. When NaOH and urea were removed, the sample was heated at 800 °C and the final product was obtained (Fig. 11(b)). Tian et al. developed a 3D porous g-C_3N_4

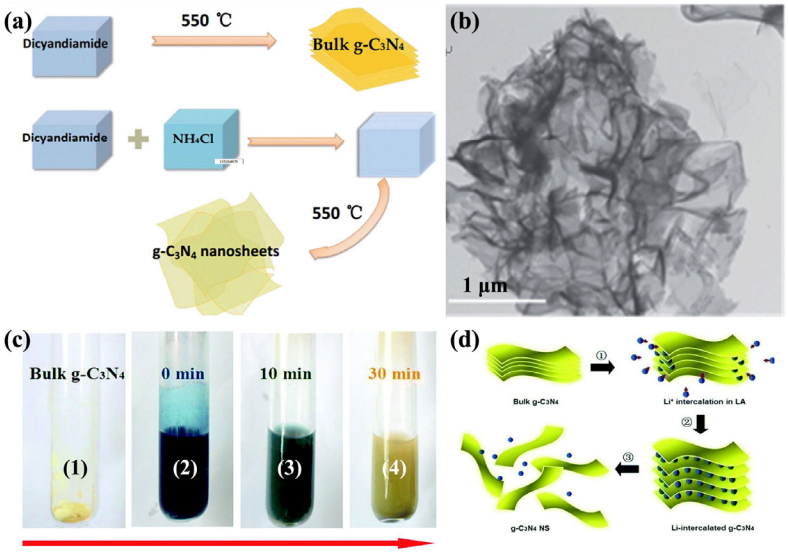

Figure 10 (a) Schematic illustration of the synthesis process of the bulk and ultrathin nanosheets of g-C_3N_4; (b) TEM image of g-C_3N_4 nanosheet (reproduced from Ref. [139] with permission, © The Royal Society of Chemistry 2014). (c) Real-time Li intercalation of bulk g-C_3N_4 in liquid ammonia; (d) schematic diagram of the lithiation and exfoliation of g-C_3N_4 nanosheets from bulk g-C_3N_4 (reproduced from Ref. [141] with permission, © The Royal Society of Chemistry 2014).

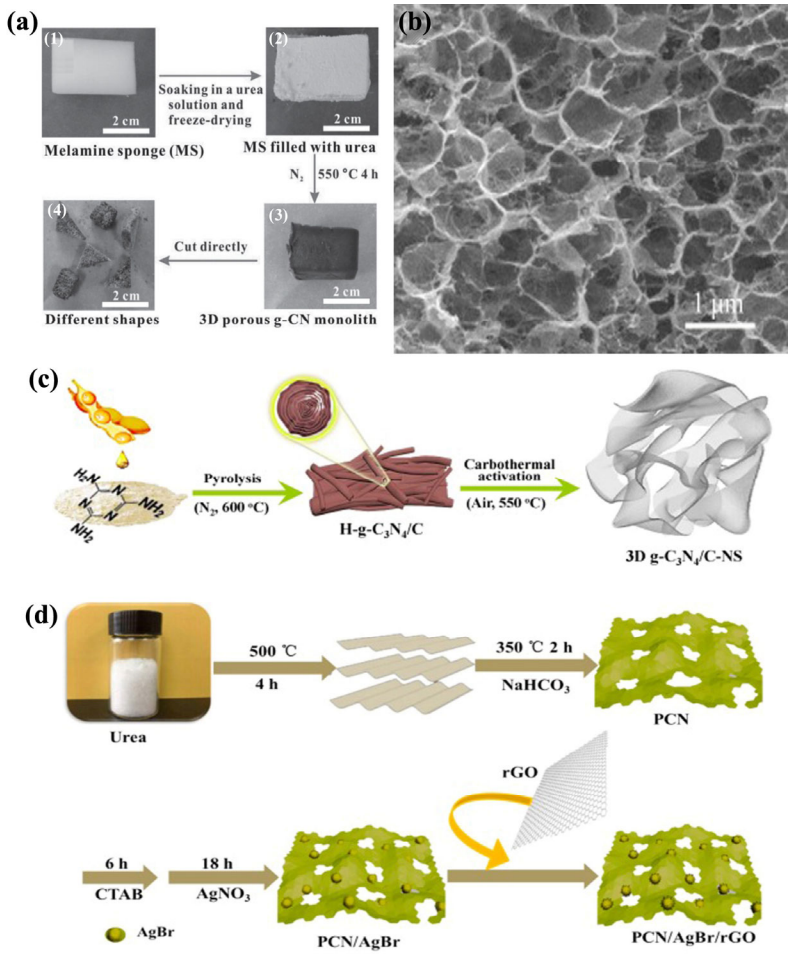

Figure 11 (a) Illustration of the preparation of a macroscopic 3D porous g-C_3N_4 monolith (reproduced from Ref. [145] with permission, © Wiley-VCH 2015). (b) SEM image of carbon/g-C_3N_4 3D network (reproduced from Ref. [146] with permission, © Elsevier Inc. 2016). (c) The synthesis process of 3D porous g-C_3N_4/C nanosheets composite (reproduced from Ref. [148] with permission, © Elsevier B.V. 2018). (d) Schematic diagrams of the preparation process of the PCN/AgBr/rGO nanocomposite (reproduced from Ref. [149] with permission, © Elsevier B.V. 2018).

by a facile and novel method [147]. They employed hydrothermal treatment to melamine and urea solution, and melamine was converted to the monoclinic phase, besides the NH_3, and CO_2 produced in the heating process were acting as porogen to create porous structure. After calcining the hydrothermal product at 520 °C for 4 h, 3D porous g-C_3N_4 with a higher apparent quantum efficiency (27.8% at 420 ± 15 nm) and superior hydrogen evolution ability was successfully fabricated. Wang

et al. prepared 3D porous g-C_3N_4/carbon nanosheets by heating the mixture of melamine and soybean oil [148]. The composite nanosheet materials had the A_{BET} of 454.2 m^2/g, which is 59.7 times as bulk g-C_3N_4, at the same time, the photocatalytic reduction CO_2 ability improved about 25 times (Fig. 11(c)). Zhou et al. used $NaHCO_3$ as porogen to create pores on bulk g-C_3N_4, leading to 3D porous net-structure [149]. Loading AgBr and reduced graphene oxide (rGO) on the 3D porous g-C_3N_4 can efficiently enhance the photocatalytic performance of g-C_3N_4 (Fig. 11(d)). Calcining the freeze-dried mixture of thiourea and sodium chloride is also an effective strategy to prepare 3D porous g-C_3N_4 [150].

3.4.2 *3D g-C_3N_4 spheres*

By employing a specific synthetic method, hollow g-C_3N_4 spheres or spheres consisting of g-C_3N_4 nanosheets can be obtained. Usually, hollow g-C_3N_4 spheres are prepared by using silica spheres as templates. Sun et al. used silica nanoparticles as a template and prepared hollow g-C_3N_4 spheres with a controllable thickness. They found that the amounts of defects increased as the thickness of the shell increased. The sample with a shell thickness of 56 nm exhibited the optimum photocatalytic performance due to its suitable length of migration path of charge carriers, a suitable amount of defects and the inner optical reflection inside the hollow spheres (Fig. 12) [151]. With the various size of silica particles, the hollow g-C_3N_4 spheres with different diameters can be obtained. All the hollow g-C_3N_4 spheres have a much higher specific surface area and can allow multiple reflections of light inside the spheres, which is helpful for its photocatalytic performance [42, 152, 153]. Coating g-C_3N_4 on the surface of hollow Pt modified TiO_2 spheres can form a structured sandwich photocatalyst with high performance on the degradation of organic pollutants [154]. Jun et al. dissolved melamine and cyanuric acid in dimethyl sulfoxide (DMSO) solution and then mixed the suspension, washed and dried it [155]. The resulted powder was heated at high temperatures, and spheres consisting of g-C_3N_4 nanosheets were achieved. With different heating temperature, the samples have different C/N ratios and different specific surface area. When the temperature is 400 °C, the obtained sample has a specific surface area of 77 m^2/g which is 12.8 times as bulk g-C_3N_4.

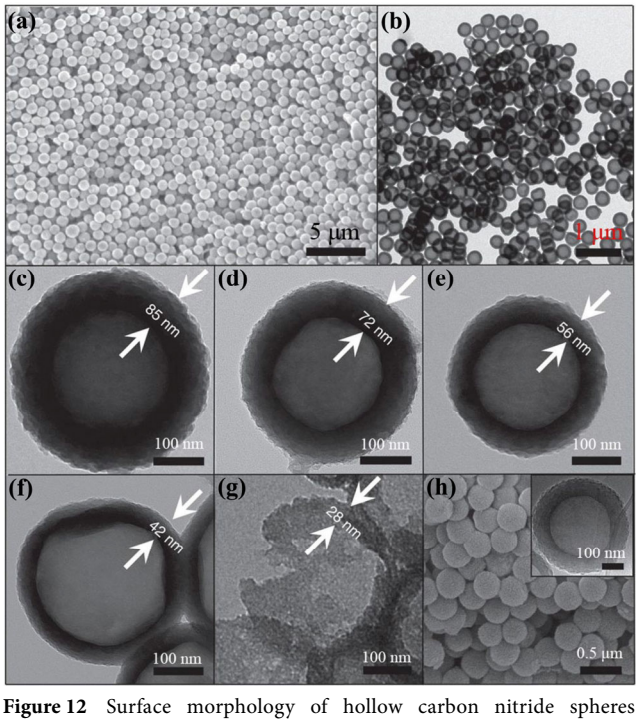

Figure 12 Surface morphology of hollow carbon nitride spheres (reproduced from Ref. [151] with permission, © Macmillan Publishers Limited 2012).

3.4.3 *3D g-C_3N_4 hydrogels*

3D hydrogels own the advantages of high adsorption capacity, good reproducibility and large specific surface area [156]. Tong et al. reported a facile synthesis of 3D g-C_3N_4/graphene oxide (GO) hydrogel by the hydrothermal reaction, and it has high performance on the photodegradation of organic pollutants (Fig. 13(a)) [157]. Wang et al. found that g-C_3N_4/graphene hydrogel also has good performance on the removal of chromium(VI) in water [158]. This group also found that the introduction of polypyrrole to g-C_3N_4/rGO hydrogel can accelerate the separation of photogenerated charge carriers [159]. Besides graphene, other materials can also form 3D hydrogels with g-C_3N_4. In our previous work, we reported the synthesis of polyacrylamide/bentonite/g-C_3N_4 3D hydrogel and its high performance in water purification (Fig. 13(b)) [12]. Zhang et al. prepared g-C_3N_4/agar and g-C_3N_4/SiO_2 and studied their synergistic effect of adsorption and photodegradation of organic pollutants (Fig. 13(c)) [160, 161]. Compared to bulk g-C_3N_4, these jelly-like 3D hydrogels have much higher adsorption ability;

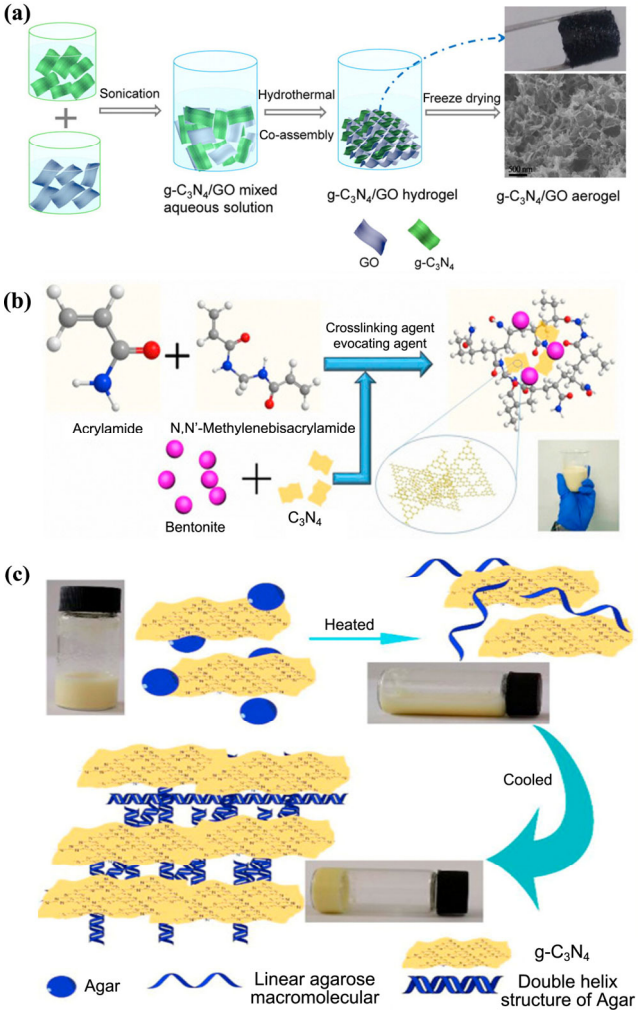

Figure 13 (a) Schematic illustration for the synthetic procedure of g-C_3N_4/graphene aerogels (reproduced from Ref. [157] with permission, © American Chemical Society 2015). (b) Preparation progress flowchart of PAM/bentonite/g-C_3N_4 3D-hydrogel (reproduced from Ref. [12] with the permission, © Elsevier B.V. 2018). (c) Schematic illustration of the preparation of C_3N_4-agar hybrid hydrogel (reproduced from Ref. [148] with permission, © Elsevier B.V. 2018).

more importantly, they are separation-free and can be recycled easily. Besides photodegradation of organic compounds, 3D g-C_3N_4 hydrogel also has application in the gas sensor. Yan et al. prepared g-C_3N_4 hydrogel by the hydrothermal reaction of g-C_3N_4 and 1-hexadecyl-3-methylimidazolium halide, which exhibited superior response on H_2S at room temperature [162]. It can also be used to detect NH_3, SO_2 and NO_2. Zhang et al. reported a 3D hydrogel network g-C_3N_4 by hydrolysing bulk g-C_3N_4 in alkaline conditions. They dissolved bulk g-C_3N_4 in NaOH solution, stirred and sonicated the suspension several times. When the concentration of NaOH was 3 M, the 3D hydrogel network g-C_3N_4 can be obtained. The synthesised network g-C_3N_4 had a high performance on the adsorption of organic dyes, such as methylene blue (MB), azure B, acriflavine and safranin O [163].

In summary, 3D g-C_3N_4 including porous 3D g-C_3N_4, 3D g-C_3N_4 spheres and 3D g-C_3N_4 hydrogels has a much larger specific surface area, higher adsorption capacity and greatly enhanced catalytic performance compared to bulk g-C_3N_4. 3D hollow g-C_3N_4 spheres or spheres consisting of g-C_3N_4 nanosheets are both 3D g-C_3N_4 spheres. In the hollow g-C_3N_4 spheres, multiple reflections of light inside spheres are the main reason for its better photocatalytic performance. For spheres consisting of g-C_3N_4 nanosheets, it has stronger optical absorption, wider bandgap and longer photogenerated-charge-carrier lifetime. Thus its catalytic activity is enhanced. Combining g-C_3N_4 with other materials can form separation-free 3D g-C_3N_4 hydrogels with multi-functions, such as adsorbent materials, photocatalysts and sensors.

3.5 Comparison of synthesis and scale of various dimensional g-C_3N_4

As shown in Table 1, the synthesis and scales of g-C_3N_4 with various dimensionalities are compared. The 0D CNQDs can be synthesised by microwave heating, solid-state reaction or chemical tailoring of bulk g-C_3N_4. In tailoring process, the strong acid and/or other strong oxidising are required, which is detrimental to the environment. Meanwhile, special protection is needed during operation to prevent safety hazards. Heating melamine and EDTA at 350 °C for 1 h can also obtain CNQDs, while the products should be dialyzed for 48 h. Therefore, microwave heating is a better option to prepare CNQDs and the process only lasts 40 s to 3 h. Besides, the diameters of microwave synthesised CNQDs are usually smaller than that achieved by tailoring method, which is between 1 to 14 nm. The synthesis of 1D g-C_3N_4 includes template method, near-infrared thermal decomposition or some special treatment. The 1D g-C_3N_4 obtained by template method has equal diameter and length. While the 1D g-C_3N_4 micro-nano rods obtained by near-infrared thermal decomposition method exhibit inhomogeneous structure. Employing acid treatment, or solvothermal reaction can change the crystal structure, crystal phase and crystal growth direction. When appropriate synthetic conditions are employed, the 1D g-C_3N_4 can be successfully synthesised. Besides, some special treatment can weaken the van der Waals' force between g-C_3N_4 layers and reassemble them into 1D structure. The post-calcined method, liquid exfoliated method or Li-ion intercalation method can also weaken the van der Waals' force between g-C_3N_4 layers and convert bulk g-C_3N_4 to 2D nanosheets. Adding additional materials to the precursors may also reduce the interlayer van der Waals' force and result in 2D nanosheets. Among these approaches, the post-calcined method is the most environmentally friendly route because it does not consume other chemicals. Heating nitrogen-rich precursors with other materials can prepare porous 3D g-C_3N_4. 3D g-C_3N_4 spheres can be obtained by template method and 3D g-C_3N_4 hydrogels are usually prepared by the polymerisation or hybridisation of other materials.

Table 1 Comparison of synthesis and scale of various dimensional g-C_3N_4

Dimension	Precursors	Synthesis	Scale	Ref.
0D	CCl_4 and EDA	Reflux, microwave, or solvothermal heating	1–5 nm	[90]
	Acid (chloro sulfonic acid (CSA), H_2SO_4, HCl, or HNO_3) and DMF	700 W microwave, 40 s	1–6 nm	[91]
	DIA, EA or TPA with acid (CSA, H_2SO_4, HCl, or HNO_3)	Microwave, 60 s	2–8 nm	[92]
	Formamide	Microwave, 180 °C, 3 h	0–14 nm	[93]
	Guanidine hydrochloride and EDTA	Microwave, 2 min	3–7 nm	[94]
	Citric acid and thiourea	700 W microwave, 7 min	2–4 nm	[95]
	Citric acid monohydrate, urea and oleic acid	180 °C for 5 min under 1,200 r/min magnetic stirring	1–5 nm	[96]
	Urea, sodium citrate	180 °C, 1 h	2–6 nm	[43]
	Bulk g-C_3N_4, H_2SO_4 and HNO_3 $NH_3{\cdot}H_2O$	Acid treatment, 2 h 180 °C, for 12 h Ultrasound in water, 6 h	2–6 nm	[97]
	Dicyandiamide, $NH_3{\cdot}H_2O$, H_2O_2	70 °C	10–15 nm	[98]
	Bulk g-C_3N_4, H_2SO_4 and HNO_3	Ultrasound in acid, 20 h	10–20 nm	[99]
	Bulk g-C_3N_4, $NaNO_3$, H_2SO_4, $KMnO_4$, H_2O_2	Treat in acid, 28 h Ultrasound in acid, 1 h	15–50 nm	[100]
	Bulk g-C_3N_4, HNO_3	Sonicate in acid, 1 h Reflux 24 h 200 °C, 12 h Sonicate in water, 4 h	1–5 nm	[101]
	Melamine, EDTA,	350 °C, 1 h Dialyze, 48 h	3–8 nm	[102]

(Continued)

Dimension	Precursors	Synthesis	Scale	Ref.
1D-rods	Cyanamide, AAO, HCl	600 °C, 2 h	*d*: 260 nm *L*: several μm	[103]
	Cyanamide, SBA-15 NH_4HF_2	550 °C, 4 h	*d*: 10 nm *L*: several μm	[104]
	SiO_2 nanorod, cyanamide, NH_4HF_2	550 °C, 4 h	*d*: 80 nm *L*: 200 nm	[105]
	Bulk g-C_3N_4, methanol–H_2O	Reflux, 3 h	*d*: 100–150 nm *L*: 0.5–3 μm	[106]
	Bulk g-C_3N_4, NH_4Cl	Sonicate for 30 min 60 °C, 12 h	*d*: 20 nm	[107]
	Thiourea, $(NH_4)_2HPO_4$ water	520 °C, 2 h 150 °C, 10 h	N/A	[108]
	Dicyandiamide	Infrared heating (50% power)	*d*: 100–500 nm *L*: several μm	[110]
	Melamine, H_2SO_4, HNO_3, and HCl	80 °C, 20 min 520 °C, 2 h	N/A	[109]
1D-tubes	Ethylenediamine, CCl_4 AAO	Reflux, 90 °C, 12 h 120 °C, 12 h 600 °C, 5 h	*d*: 300 nm Thickness: 30 nm *L*: several μm	[114]
	$C_3N_3Cl_3$, melamine	Low-pressure desorption, 24 h 800 °C, 2 h	*d*: 0.5–5 μm Thickness: 200–250 nm *L*: tens of μm	[115]
	$NiCl_2$, cyclohexane, Na $C_3N_3Cl_3$	230 °C, 6 h 230 °C, 10 h	*d*: 50–100 nm Thickness: 17 nm *L*: N/A	[116]
	Melamine, phosphorous acid	Stir, 30 min 180 °C, 10 h 500 °C, 4 h	*d*: 60–100 μm Thickness: N/A *L*: 300–500 μm	[118]
	Melamine	200 °C, 24 h 550 °C, 4 h	*d*: 80 nm Thickness: 12 nm *L*: N/A	[119]
	Cyanuric acid, melamine, caffeine	500 °C	N/A	[117]
1D-wires	Melamine, ethanol, HNO_3	450 °C, 2 h	*d*: 100 nm *L*: 20 μm	[120]
	Cyanuric chloride, melamine	Stir 12 h, 180 °C, 24 h	*d*: 20–30 nm *L*: hundreds μm	[121]
	Dicyandiamide,	200 °C, 4 h Freeze-dried at 500–650 °C	*d*: about 500 nm *L*: N/A	[164]
	Melamine, hydroiodic acid H_2O_2 H_2O_2 and C_2H_5OH	550 °C, 5 h 180 °C, 12 h Self-assembly in solution, 12 h	*d*: 100 nm *L*: N/A	[123]
2D	Bulk g-C_3N_4	Grind, 500 °C, 2 h	Thickness: 1.65–2.62 nm	[124]
	Bulk g-C_3N_4	520 °C, 6 h	Thickness: 9.2 nm	[125]
	Bulk g-C_3N_4	Ultrasound in water, 16 h	Thickness: 2.5 nm	[127]
	Melamine, IPA	520 °C, 4 h 550 °C, 3 h Ultrasound in IPA, 8 h	Thickness: 0.5 nm	[133]
	Bulk g-C_3N_4, H_2SO_4	Stir in acid, 8 h	Thickness: 0.4 nm	[132]
	Dicyandiamide, lithium chloride and potassium chloride	400 °C, 6 h 600 °C, 12 h	Hexagonal, 100–200 nm	[136]
	Melamine, KBH_4	550 °C, 4 h	Thickness: 1.5 nm	[137]
	Dicyandiamide, NH_3Cl	550 °C, 4 h	Thickness: 3.2 nm	[139]
	Melamine, cyanuric acid	550 °C, 4 h	N/A	[140]
	Bulk g-C_3N_4, liquid ammonia, Li	Ultrasound in solution, 30 min	Thickness: 2.5 nm	[141]
	Melamine, carbon fibre	Microwave, 5 kW, 5 min	Thickness: 1.6 nm	[142]
Porous 3D g-C_3N_4	Melamine hydrochloride	500 °C, 2 h 520 °C, 2 h		[144]
	Melamine sponge, urea	550 °C, 2 h		[145]
	Urea, chitin, NaOH and g-C_3N_4	freeze and thaw 800 °C, 2 h		[146]
	Melamine, urea	180 °C, 24 h 520 °C, 4 h		[147]

(Continued)

Dimension	Precursors	Synthesis	Scale	Ref.
	Melamine, soybean oil	600 °C, 2 h		[148]
	Urea $NaHCO_3$	500 °C, 4 h 350 °C, 2 h		[149]
	Thiourea, sodium chloride	Freeze dry 500 °C, 0.5 h		[150]
3D g-C_3N_4 spheres	SiO_2, cyanamide	Mix, 3 h 550 °C, 4 h	Hollow sphere Thickness: 56 nm	[151]
	Cyanamide, barbituric acid, SiO_2	550 °C, 4 h	*d*: 20 nm	138
	Melamine, cyanuric acid, DMSO	400 °C, 4 h	*d*: 2 μm	[155]
3D g-C_3N_4 hydrogels	Bulk g-C_3N_4, rGO	180 °C, 6 h		[157]
	Cyanurotriamide, GO, sodium ascorbate	550 °C, 4 h 95 °C, 1 h		[158]
	Bulk g-C_3N_4, ppy-rGO	Ultrasound, 2 h		[159]
	g-C_3N_4, Polyacrylamide, bentonite	Polymerization		[12]
	Bulk g-C_3N_4, SiO_2 NaOH, HCl	Hybridization		[160]
	Bulk g-C_3N_4, agar	95 °C, 5 min		[161]
	Bulk g-C_3N_4, 1-hexadecyl-3-methylimidazolium halide	200 °C, 24 h Quick cool		[162]
	Bulk g-C_3N_4, NaOH	60 °C, 12 h and ultrasound for 1 h every 4 h		[163]

4 Energy and environmental application of various dimensional g-C_3N_4

The dimensions of materials can affect their surface area, layer stacking method, transfer paths and separation ratios of electron and hole pairs, and therefore, their properties in different aspects are entirely different. As shown in Table 2, the applications of g-C_3N_4 with various dimensionalities are summarised and compared.

CNQDs are 0D materials with wide energy and environmental application. Due to the tri-s-triazine unit, g-C_3N_4 shows strong luminescent and chemical stability. The strong emission and large exciton binding energy can make g-C_3N_4 show stable high-yield luminescence [178]. The luminescent properties of quantum dots are caused by the interaction of electrons, holes and their surroundings [179]. When the excitation energy exceeds the band gap, the g-C_3N_4 quantum dots can absorb photons, creating electron–hole pairs. Most excited electrons can recombine with holes and cause strong fluorescence. At the same time, the transition of triplet excited state electrons can lead to phosphorescence [180]. For the quantum confinement effect, the size of CNQDs can control its band gap, and therefore CNQDs have regulatable spectrum [181]. More importantly, the broad Stokes shift of CNQDs can avoid the overlap of the emission spectrum and excitation spectrum, which is beneficial to the detection of fluorescence spectrum signals [182]. Thus the application of CNQDs is mainly based on its excellent fluorescence property, for example, CNQDs can be used as sensors to detect glucose [92], H_2O_2 [92], mercuric ions [93], iodide ions [93], free residual chlorine [94], iron ion [167], glutathione [165], and dopamine (Fig. 4(c)) [102]. The g-CNQDs emerge as a novel fluorescent probe for biological and environment detection with unique physicochemical properties. As an ideal fluorescent probe, its fluorescence could be completely and specifically quenched by Hg^{2+}, thus it can be a good sensor of Hg^{2+}. Figure 14(a) shows the principle of the g-CNQDs-Hg^{2+} system based chemosensor for glutathione. The original fluorescence of g-CNQDs was quenched after the addition of Hg^{2+}. After the addition of glutathione, Hg^{2+} was strongly captured by glutathione and released from the surface of g-CNQDs, as a result, high intensity of fluorescence can be detected [152]. Besides, CNQDs also have excellent performance in catalytic materials. It can improve the catalytic activity of electrocatalysts [100], photocatalysts [166, 183] and photoelectric catalysts [169, 184]. Meanwhile, it has good photocatalytic activity [98]. Furthermore, it can be used to improve the efficiency of heterojunction polymer solar cells [99].

The 1D g-C_3N_4, including g-C_3N_4 micro-nano rods, g-C_3N_4 micro-nano tubes and g-C_3N_4 micro-nano wires, has a large surface area and strong conductivity. Besides, for the 1D structure, photogenerated charge carriers can rapidly transfer to the surface of g-C_3N_4 and the recombination of electron–hole pairs is minimised. More importantly, in some 1D synthesis, the precursors or bulk g-C_3N_4 were treated in liquid, which can change the crystal growth, improve the crystallinity and passivate surface defects. Thus, 1D g-C_3N_4 has unique performance in photocatalysis, including water splitting and organic pollutant degradation. For instance, Zhang et al. prepared g-C_3N_4 micro-nano wires with tunable bandgap and unique overall water splitting performance. As shown in Fig. 14(b), the band gap of bulk g-C_3N_4 is 2.63 eV and it is 2.71 eV for g-C_3N_4 micro-nano wires. Interestingly, a mid-gap state occurred to the structure of g-C_3N_4 micro-nano wires and the band gap was divided into two parts, resulting in the multiple electronic transitions. The mid-gap state and the unique 1D structure can significantly accelerate the transfer and separation of electron–hole pairs. As a result, the photocatalytic performance of g-C_3N_4 micro-nano wires was improved significantly [109]. The hollow structured g-C_3N_4 micro-nano tube can be used as catalyst carriers to achieve more catalytic reactions. By contrast, 1D g-C_3N_4 usually has low luminescence, thus is not suitable for the luminescent application.

Compared to bulk g-C_3N_4, 2D g-C_3N_4 has a much higher surface area and better optical property. The broadest application

Table 2 Comparison of the application of various dimensional g-C_3N_4

Materials	Application classification	Application	Ref.
CNQDs	Environmental	Detection of Hg^{2+} and I^-	[93]
	Environmental	Detection of glucose and H_2O_2	[92]
	Environmental	Detection of free chlorine	[94]
	Environmental	Detection of dopamine	[102]
	Environmental	Detection of glutathione	[165]
	Environmental	Photodegradation of RhB	[166]
	Environmental	Detection of Fe^{3+}	[167]
	Environmental	Photoelectrodegradation of phenol	[168]
	Energy	Photocatalytic H_2 generation	[98]
	Energy	ORR	[100]
	Energy	Photoelectrochemical water splitting	[169]
	Energy	Polymer solar cells	[99]
Rods	Environmental	Photodegradation of MB	[106]
	Environmental	Photodegradation of RhB	[108]
	Environmental	Photoelectrochemical Sensing of Cu^{2+}	[107]
	Energy	Photocatalytic water splitting	[103]
	Energy	Photocatalytic H_2 generation	[105]
Tubes	Environmental	Catalytic cyclohexene hydrogenation	[114]
	Environmental	Photodegradation of RhB	[119]
	Energy	Photocatalytic H_2 generation	[118]
Wires	Environmental	Photodegradation of RhB	[120]
	Environmental	Adsorption and photodegradation of MB	[121]
	Energy	Photocatalytic water splitting	[123]
Sheets	Environmental	Photodegradation of RhB	[66]
	Environmental	Photodegradation of tetracycline	[170]
	Environmental	Photodegradation of 2,4-dichlorophenol	[171]
	Environmental	Photocatalytic reduction of NO	[140]
	Environmental	Sterilization	[172]
	Environmental	Self-cleaning	[173]
	Environmental	Detection of Cu^{2+}	[174]
	Environmental	Detection of Hg^{2+} and Fe^{3+}	[175]
	Energy	Photocatalytic water splitting	[135]
	Energy	Photocatalytic reduction of CO_2	[176]
Porous	Environmental	Photodegradation of RhB	[144]
	Environmental	Photodegradation of 2,4-DCP	[149]
	Energy	ORR, OER	[146]
	Energy	Photocatalytic reduction of CO_2	[148]
	Energy	Photocatalytic H_2 generation	[145]
Spheres	Environmental	Photodegradation of phenol	[42]
	Environmental	Photodegradation of RhB	[154]
	Energy	Photocatalytic H_2 generation	[151]
	Energy	Photocatalytic reduction of CO_2	[177]
Hydrogels	Environmental	Adsorption and photodegradation MO	[157]
	Environmental	Adsorption and photodegradation MB	[160]
	Environmental	Adsorption and photocatalytic removal of Cr^{6+}	[158]
	Environmental	Adsorption and photodegradation tetracycline	[12]
	Environmental	Gas-sensor	[162]

of 2D g-C_3N_4 is in the area of photocatalysts. With the band gap of 2.7 eV, g-C_3N_4 can be excited by visible light. Niu et al. used g-C_3N_4 nanosheets to split water and generate hydrogen [129]. The photocatalytic reduction reaction of g-C_3N_4 nanosheets can convert CO_2 to useful fuels [176]. Xia et al. obtained ultra-thin g-C_3N_4 nanosheets by heating bulk g-C_3N_4 in NH_3 atmosphere [23]. As shown in Fig. 14(c), the adsorption energy of CO_2 molecules on bulk g-C_3N_4 is −0.99 eV, and it can be reduced to −1.37 eV on the surface of g-C_3N_4 nanosheet, which is beneficial for photocatalytic CO_2 conversion. Besides, the higher specific surface area makes the g-C_3N_4 nanosheet have larger number of active sites and enhanced photocatalytic activity. Besides, g-C_3N_4 nanosheets can also photodegrade organic pollutants such as phenol, rhodamine B (RhB), tetracycline or 2,4-dichlorophenol [12, 66, 170, 171]. The photocatalytic oxidation reaction of g-C_3N_4 nanosheets can also be applied in sterilisation and self-cleaning [172, 173]. At the same time, g-C_3N_4 nanosheets have strong luminesce and have excellent performance in fluorescent sensors [174, 175].

The 3D porous g-C_3N_4 can be used in photocatalytic oxidation, photocatalytic reduction and electrocatalytic reaction. For the porous structure, the 3D porous g-C_3N_4 usually has a large surface area that results in high performance. In 3D g-C_3N_4 spheres, multiple reflections of light inside spheres make them have excellent photocatalytic performance in both organic pollutant oxidisation and fuel generation. As for 3D g-C_3N_4 hydrogels, it has both adsorption and photocatalytic ability. Thus its synergistic effect is always adopted to purify wastewater. Figure 14(d) is the mechanism for the adsorption and degradation of tetracycline over g-C_3N_4 based hydrogel. When polluted water flows through the hydrogel, the pollutants can be adsorbed on the hydrogel. Meanwhile, the strong oxidising species, produced by g-C_3N_4 under visible light irradiation can mineralise the organic pollutants into CO_2 and H_2O. As a result, the composite hydrogel remains in dynamic equilibrium, for continuous wastewater purification. The enhanced photocatalytic activity is attributed to the strong light absorption and accelerated the separation of photogenerated charge carriers [12]. Besides, it can also be used as a gas sensor.

5 Summary and outlook

In recent years, g-C_3N_4 based materials have attracted increasing attention for its excellent properties, such as high stability, nontoxicity, facile and low-cost synthesis, visible light absorption and wide resources. In energy and environmental areas, g-C_3N_4 has broad application prospects. For example, the photocatalytic reduction reaction of g-C_3N_4 can be used for water splitting, which generates hydrogen as zero-emission fuel with much higher calorific value compared to fossil fuels. Photoreduction of CO_2 is an efficient approach to reduce the circumstance of global warming because it can convert CO_2 to useful organic molecules such as methane, methanol, ethylene, etc. Photocatalytic oxidation reaction can be used in mineralising organic pollutants in water, sterilisation and self-cleaning materials. The luminescence of g-C_3N_4 empowers its application in the fluorescence detection of heavy metallic ions in water.

The strong emission and large exciton binding energy enable g-C_3N_4 to exhibit stable high-yield luminescence [178]. The luminescent properties of quantum dots are caused by the interaction of electrons, holes and their surroundings [179]. When the excitation level exceeds the band gap, the quantum dots absorb photons and make the transition from the valence band to the conduction band. Most excited electrons can recombine with holes and cause strong fluorescence and the

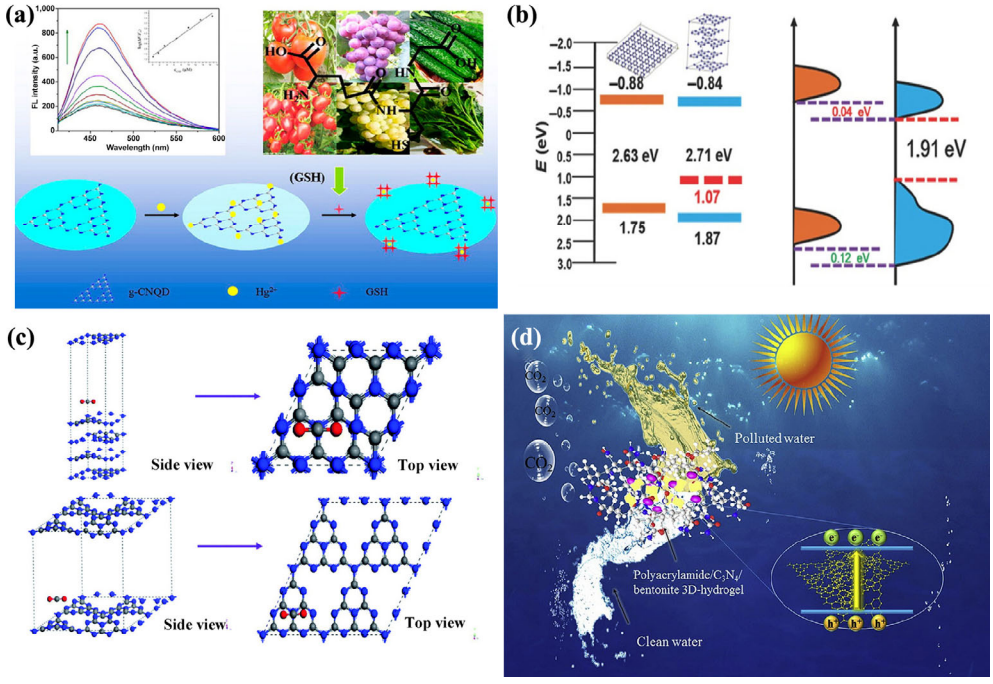

Figure 14 (a) The principle of the g-CNQDs-Hg^{2+} system based chemosensor for glutathione (reproduced from Ref. [165] with permission, © American Chemical Society 2015). (b) The calculated bandgap and density of states (DOS) of g-C_3N_4 and g-C_3N_4 nanowires (reproduced from Ref. [123] with permission, © Wiley-VCH 2016). (c) The optimised configurations of a single CO_2 molecule adsorbed on the surface of bulk g-C_3N_4 and g-C_3N_4 nanosheets based on density functional theory (DFT) calculations (reproduced from Ref. [22] with permission, © The Royal Society of Chemistry 2017). (d) The mechanism for the adsorption and degradation of tetracycline over polyacrylamide/bentonite/g-C_3N_4 (PAM/B/CN) hydrogel (reproduced from Ref. [12] with permission, © Elsevier Ltd. 2018).

optical transition in lone-pair electronic states can cause phosphorescence [180]. For the quantum confinement effect, the size of CNQDs can be controlled to regulate its band gap and spectrum [181]. More importantly, the large Stokes shift of CNQDs can avoid the overlap of the emission spectrum and excitation spectrum, which is beneficial to the detection of fluorescence spectrum signals [182]. 0D g-C_3N_4 can be prepared by microwave-assisted synthesis, solid state reaction and chemical tailor of bulk g-C_3N_4; and the application of CNQDs is mainly based on its excellent fluorescence property. It can be used as sensors to detect heavy metallic ions and other hazardous molecules. 1D g-C_3N_4 includes g-C_3N_4 rods, g-C_3N_4 tubes and g-C_3N_4 wires, in which electrons have free movement in the direction of material extension. As a result, the separation efficiency of photogenerated charge carriers are promoted significantly, thus 1D g-C_3N_4 is most applied as photocatalysts. By contrast, 1D g-C_3N_4 usually has low luminescence and is not suitable for the luminescent application. 1D g-C_3N_4 is usually synthesised by CVD, template method, or solvent and thermal treatment of bulk g-C_3N_4. The electrons in 2D g-C_3N_4 can move freely in two dimensions. Compared with bulk g-C_3N_4, 2D g-C_3N_4 has a much higher specific surface area, better optical property and thus enhanced performance in different aspects, such as photocatalysts, sensors, sterilisation and self-cleaning. 2D g-C_3N_4 can be synthesised by post-calcined method, liquid exfoliated method and other ways. 3D g-C_3N_4 includes porous 3D g-C_3N_4, 3D g-C_3N_4 spheres and 3D g-C_3N_4 hydrogels. Porous 3D g-C_3N_4 can be prepared by heating melamine hydrochloride, sponge-assisted method, precursor-reforming protocol et al. 3D g-C_3N_4 spheres can be obtained by template method, while 3D g-C_3N_4 hydrogels should be prepared during the polymerisation process of other materials.

For the excellent property and low-cost preparation, g-C_3N_4 is likely to be applied in future industrial energy and environmental areas. In order to achieve this goal, some aspects still need to be accomplished. (1) Due to the quantum confinement effect, the diameters of CNQDs have great influence on their band gap and spectrum, thus different CNQDs with different diameters have different properties and application. It is necessary to control the quantum size effect by accurately controlling the size of CNQDs. Controlling the temperature, pressure and time can help control the size, while it still needs exploration. (2) For the 1D electronic confined effect, recombination of electron–hole pairs can be minimised and it has broad prospects in the catalytic area. However, the synthetic approaches usually involve the template or re-crystallisation, which need complex steps and are not environmentally friendly. It remains uncertain if 1D g-C_3N_4 can be produced more easily and if the problems of high energy consumption and pollution can be avoided in the production process of 1D g-C_3N_4. (3) Although many strategies for weakening the van der Waals force between the g-C_3N_4 are mentioned here, it is very difficult to keep the nanolayers stable. How to inhibit the stacking of layers and improve the stability of two-dimensional nanosheets is still a subject worth studying. 3D g-C_3N_4 hydrogels, surface modification and ion intercalation can help to inhibit its stacking. (4) 2D g-C_3N_4 nanosheets come from bulk g-C_3N_4 but the synthesis of bulk g-C_3N_4 usually produces a large amount of end gas (ammonia). If the end gas can be collected and converted to useful matter, the production process can be green and eco-friendly. (5) Nowadays, the main research focuses on the synergism of adsorption and photocatalytic degradation of pollutants. The 3D g-C_3N_4 hydrogels can overcome several drawbacks of bulk g-C_3N_4 and can even come into some unexpected properties. It is still urgent to develop new types of 3D g-C_3N_4 hydrogels and expand their application scopes.

The g-C_3N_4 is an amazing material with a broad prospect in energy and environmental areas. However, it is usually bulk structure and micro scale, which limits the transfer of electrons and limits its performance. With the bandgap of 2.7 eV, its solar

energy utilization ratio is not high. As opportunities come with challenges, tremendous efforts are required to improve its property before it can be applied in many stimulating applications to make our planet better.

Acknowledgements

This work is supported by an Australian Research Council (ARC) Future Fellowship (No. FT160100195). G. H. J. acknowledges the support from the Australian Research Council (ARC) Discovery Early Career Researcher Award (ARC DECRA) (Project ID: DE160100589). Q. H. acknowledges the technical support of Beijing NBET Technology Co., Ltd.

References

[1] Yu, Z. N.; Tetard, L.; Zhai, L.; Thomas, J. Supercapacitor electrode materials: Nanostructures from 0 to 3 dimensions. *Energy Environ. Sci.* **2015**, *8*, 702–730.

[2] Pokropivny, V. V.; Skorokhod, V. V. Classification of nanostructures by dimensionality and concept of surface forms engineering in nanomaterial science. *Mater. Sci. Eng. C* **2007**, *27*, 990–993.

[3] Gu, W.; Yan, Y. H.; Pei, X. Y.; Zhang, C. L.; Ding, C. P.; Xian, Y. Z. Fluorescent black phosphorus quantum dots as label-free sensing probes for evaluation of acetylcholinesterase activity. *Sens. Actuators B: Chem.* **2017**, *250*, 601–607.

[4] Yuan, F. L.; Wang, Z. B.; Li, X. H.; Li, Y. C.; Tan, Z. A.; Fan, L. Z.; Yang, S. H. Bright multicolor bandgap fluorescent carbon quantum dots for electroluminescent light-emitting diodes. *Adv. Mater.* **2017**, *29*, 1604436.

[5] Kroupa, D. M.; Hughes, B. K.; Miller, E. M.; Moore, D. T.; Anderson, N. C.; Chernomordik, B. D.; Nozik, A. J.; Beard, M. C. Synthesis and spectroscopy of silver-doped PbSe quantum dots. *J. Am. Chem. Soc.* **2017**, *139*, 10382–10394.

[6] Hou, L. Z.; Mead, J. L.; Wang, S. L.; Huang, H. The kinetic frictional shear stress of ZnO nanowires on graphite and mica substrates. *Appl. Surf. Sci.* **2018**, *465*, 584–590.

[7] Yu, L.; Zhou, H. Q.; Sun, J. Y.; Qin, F.; Yu, F.; Bao, J. M.; Yu, Y.; Chen, S.; Ren, Z. F. Cu nanowires shelled with NiFe layered double hydroxide nanosheets as bifunctional electrocatalysts for overall water splitting. *Energy Environ. Sci.* **2017**, *10*, 1820–1827.

[8] Qiu, C. G.; Zhang, Z. Y.; Xiao, M. M.; Yang, Y. J.; Zhong, D. L.; Peng, L. M. Scaling carbon nanotube complementary transistors to 5-nm gate lengths. *Science* **2017**, *355*, 271–276.

[9] Ge, M. Z.; Li, Q. S.; Cao, C. Y.; Huang, J. Y.; Li, S. H.; Zhang, S. N.; Chen, Z.; Zhang, K. Q.; Al-Deyab, S. S.; Lai, Y. K. One-dimensional TiO_2 nanotube photocatalysts for solar water splitting. *Adv. Sci.* **2017**, *4*, 1600152.

[10] Pei, L.; Lv, B. H.; Wang, S. B.; Yu, Z. T.; Yan, S. C.; Abe, R.; Zou, Z. G. Oriented growth of Sc-doped Ta_3N_5 nanorod photoanode achieving low-onset-potential for photoelectrochemical water oxidation. *ACS Appl. Energy Mater.* **2018**, *1*, 4150–4157.

[11] Li, X. Y.; Li, D.; Tian, H.; Zeng, L.; Zhao, Z. J.; Gong, J. L. Dry reforming of methane over Ni/La_2O_3 nanorod catalysts with stabilized Ni nanoparticles. *Appl. Catal. B: Environ.* **2017**, *202*, 683–694.

[12] Hao, Q.; Chen, T.; Wang, R. T.; Feng, J. R.; Chen, D. M.; Yao, W. Q. A separation-free polyacrylamide/bentonite/graphitic carbon nitride hydrogel with excellent performance in water treatment. *J. Clean. Prod.* **2018**, *197*, 1222–1230.

[13] Novoselov, K. S.; Mishchenko, A.; Carvalho, A.; Neto, A. H. C. 2D materials and van der Waals heterostructures. *Science* **2016**, *353*, aac9439.

[14] Liao, S. H.; Jhuo, H. J.; Cheng, Y. S.; Chen, S. A. Fullerene derivative-doped zinc oxide nanofilm as the cathode of inverted polymer solar cells with low-bandgap polymer (PTB7-Th) for high performance. *Adv. Mater.* **2013**, *25*, 4766–4771.

[15] Sun, Z. P.; Martinez, A.; Wang, F. Optical modulators with 2D layered materials. *Nat. Photonics* **2016**, *10*, 227–238.

[16] Erdoğan, I. Y.; Güllü, Ö. Optical and structural properties of CuO nanofilm: Its diode application. *J. Alloys Compd.* **2010**, *492*, 378–383.

[17] Wang, X.; Tian, W.; Liao, M. Y.; Bando, Y.; Golberg, D. Recent advances in solution-processed inorganic nanofilm photodetectors. *Chem. Soc. Rev.* **2014**, *43*, 1400–1422.

[18] Du, M. S.; Cui, L. S.; Cao, Y.; Bard, A. J. Mechanoelectrochemical catalysis of the effect of elastic strain on a platinum nanofilm for the ORR exerted by a shape memory alloy substrate. *J. Am. Chem. Soc.* **2015**, *137*, 7397–7403.

[19] Hao, Q.; Niu, X. X.; Nie, C. S.; Hao, S. M.; Zou, W.; Ge, J. M.; Chen, D. M.; Yao, W. Q. A highly efficient g-C_3N_4/SiO_2 heterojunction: The role of SiO_2 in the enhancement of visible light photocatalytic activity. *Phys. Chem. Chem. Phys.* **2016**, *18*, 31410–31418.

[20] Hao, Q.; Hao, S. M.; Niu, X. X.; Li, X.; Chen, D. M.; Ding, H. Enhanced photochemical oxidation ability of carbon nitride by π–π stacking interactions with graphene. *Chin. J. Catal.* **2017**, *38*, 278–286.

[21] Ersan, G.; Apul, O. G.; Perreault, F.; Karanfil, T. Adsorption of organic contaminants by graphene nanosheets: A review. *Water Res.* **2017**, *126*, 385–398.

[22] Xia, P. F.; Zhu, B. C.; Yu, J. G.; Cao, S. W.; Jaroniec, M. Ultra-thin nanosheet assemblies of graphitic carbon nitride for enhanced photocatalytic CO_2 reduction. *J. Mater. Chem. A* **2017**, *5*, 3230–3238.

[23] Park, J.; Mangeri, J.; Zhang, Q. T.; Yusuf, M. H.; Pateras, A.; Dawber, M.; Holt, M. V.; Heinonen, O. G.; Nakhmanson, S.; Evans, P. G. Domain alignment within ferroelectric/dielectric $PbTiO_3$/$SrTiO_3$ superlattice nanostructures. *Nanoscale* **2018**, *10*, 3262–3271.

[24] Khayyami, A.; Karppinen, M. Reversible photoswitching function in atomic/molecular-layer-deposited ZnO:azobenzene superlattice thin films. *Chem. Mater.* **2018**, *30*, 5904–5911.

[25] Tayari, V.; Hemsworth, N.; Fakih, I.; Favron, A.; Gaufrès, E.; Gervais, G.; Martel, R.; Szkopek, T. Two-dimensional magnetotransport in a black phosphorus naked quantum well. *Nat. Commun.* **2015**, *6*, 7702.

[26] Freundlich, A.; Alemu, A. Multi quantum well multijunction solar cell for space applications. *Phys. Status Solidi (C)* **2005**, *2*, 2978–2981.

[27] Guo, F.; Creighton, M.; Chen, Y. T.; Hurt, R.; Külaots, I. Porous structures in stacked, crumpled and pillared graphene-based 3D materials. *Carbon* **2014**, *66*, 476–484.

[28] Silveira, J. F. R. V.; Muniz, A. R. Diamond nanothread-based 2D and 3D materials: Diamond nanomeshes and nanofoams. *Carbon* **2018**, *139*, 789–800.

[29] Yu, H. J.; Shi, R.; Zhao, Y. X.; Bian, T.; Zhao, Y. F.; Zhou, C.; Waterhouse, G. I. N.; Wu, L. Z.; Tung, C. H.; Zhang, T. R. Alkali-assisted synthesis of nitrogen deficient graphitic carbon nitride with tunable band structures for efficient visible-light-driven hydrogen evolution. *Adv. Mater.* **2017**, *29*, 1605148.

[30] Wang, X. S.; Zhou, C.; Shi, R.; Liu, Q. Q.; Waterhouse, G. I. N.; Wu, L. Z.; Tung, C. H.; Zhang, T. R. Supramolecular precursor strategy for the synthesis of holey graphitic carbon nitride nanotubes with enhanced photocatalytic hydrogen evolution performance. *Nano Res.* **2019**, *12*, 2385–2389.

[31] Zhou, C.; Shi, R.; Shang, L.; Wu, L. Z.; Tung, C. H.; Zhang, T. R. Template-free large-scale synthesis of g-C_3N_4 microtubes for enhanced visible light-driven photocatalytic H_2 production. *Nano Res.* **2018**, *11*, 3462–3468.

[32] Zhao, H.; Ding, X. L.; Zhang, B.; Li, Y. X.; Wang, C. Y. Enhanced photocatalytic hydrogen evolution along with byproducts suppressing over Z-scheme $Cd_xZn_{1-x}S$/Au/g-C_3N_4 photocatalysts under visible light. *Sci. Bull.* **2017**, *62*, 602–609.

[33] Liebig, J. About some nitrogen compounds. *Ann. Pharm.* **1834**, *10*, 10.

[34] Zhou, Z. X.; Zhang, Y. Y.; Shen, Y. F.; Liu, S. Q.; Zhang, Y. J. Molecular engineering of polymeric carbon nitride: Advancing applications from photocatalysis to biosensing and more. *Chem. Soc. Rev.* **2018**, *47*, 2298–2321.

[35] Franklin, E. C. The ammono carbonic acids. *J. Am. Chem. Soc.* **1922**, *44*, 486–509.

[36] Liu, A. Y.; Cohen, M. L. Prediction of new low compressibility solids. *Science* **1989**, *245*, 841–842.

[37] Teter, D. M.; Hemley, R. J. Low-compressibility carbon nitrides. *Science* **1996**, *271*, 53–55.

[38] Zhang, J. S.; Wang, B.; Wang, X. C. Chemical synthesis and applications of graphitic carbon nitride. *Acta Phys. Chim. Sin.* **2013**, *29*, 1865–1876.

[39] Molina, B.; Sansores, L. E. Electronic structure of six phases of C_3N_4: A theoretical approach. *Mod. Phys. Lett. B* **1999**, *13*, 193–201.

[40] Kroke, E.; Schwarz, M.; Horath-Bordon, E.; Kroll, P.; Noll, B.; Norman, A. D. Tri-s-triazine derivatives. Part I. From trichloro-tri-s-

triazine to graphitic C_3N_4 structures. *New J. Chem.* **2002**, *26*, 508–512.
[41] Hao, Q.; Xie, C. A.; Huang, Y. M.; Chen, D. M.; Liu, Y. W.; Wei. W.; Ni, B. J. Accelerated separation of photogenerated charge carriers and enhanced photocatalytic performance of g-C_3N_4 by Bi_2S_3 nanoparticles. *Chin. J. Catal.* **2020**, *41*, 249–258.
[42] Li, Y. D.; Ruan, Z. H.; He, Y. Z.; Li, J. Z.; Li, K. Q.; Yang, Y. L.; Xia, D. B.; Lin, K. F.; Yuan, Y. Enhanced photocatalytic H_2 evolution and phenol degradation over sulfur doped meso/macroporous g-C_3N_4 spheres with continuous channels. *Int. J. Hydrogen Energy* **2019**, *44*, 707–719.
[43] Zhou, J.; Yang, Y.; Zhang, C. Y. A low-temperature solid-phase method to synthesize highly fluorescent carbon nitride dots with tunable emission. *Chem. Commun.* **2013**, *49*, 8605–8607.
[44] Mishra, A.; Mehta, A.; Basu, S.; Shetti, N. P.; Reddy, K. R.; Aminabhavi, T. M. Graphitic carbon nitride (g-C_3N_4)-based metal-free photocatalysts for water splitting: A review. *Carbon* **2019**, *149*, 693–721.
[45] Wen, J. Q.; Xie, J.; Chen, X. B.; Li, X. A review on g-C_3N_4-based photocatalysts. *Appl. Surf. Sci.* **2017**, *391*, 72–123.
[46] Zhang, S.; Gu, P. C.; Ma, R.; Luo, C. T.; Wen, T.; Zhao, G. X.; Cheng, W. C.; Wang, X. K. Recent developments in fabrication and structure regulation of visible-light-driven g-C_3N_4-based photocatalysts towards water purification: A critical review. *Catal. Today* **2019**, *335*, 65–77.
[47] Cao, S. W.; Yu, J. G. g-C_3N_4-based photocatalysts for hydrogen generation. *J. Phys. Chem. Lett.* **2014**, *5*, 2101–2107.
[48] Cao, S. W.; Low, J. X.; Yu, J. G.; Jaroniec, M. Polymeric photocatalysts based on graphitic carbon nitride. *Adv. Mater.* **2015**, *27*, 2150–2176.
[49] Ren, Y. J.; Zeng, D. Q.; Ong, W. J. Interfacial engineering of graphitic carbon nitride (g-C_3N_4)-based metal sulfide heterojunction photocatalysts for energy conversion: A review. *Chin. J. Catal.* **2019**, *40*, 289–319.
[50] Nikokavoura, A.; Trapalis, C. Graphene and g-C_3N_4 based photocatalysts for NO_x removal: A review. *Appl. Surf. Sci.* **2018**, *430*, 18–52.
[51] Masih, D.; Ma, Y. Y.; Rohani, S. Graphitic C_3N_4 based noble-metal-free photocatalyst systems: A review. *Appl. Catal. B*: *Environ.* **2017**, *206*, 556–588.
[52] Zhang, C.; Li, Y.; Shuai, D. M.; Shen, Y.; Xiong, W.; Wang, L. Q. Graphitic carbon nitride (g-C_3N_4)-based photocatalysts for water disinfection and microbial control: A review. *Chemosphere* **2019**, *214*, 462–479.
[53] Fu, J. W.; Yu, J. G.; Jiang, C. J.; Cheng, B. g-C_3N_4-based heterostructured photocatalysts. *Adv. Energy Mater.* **2018**, *8*, 1701503.
[54] Jiang, L. B.; Yuan, X. Z.; Pan, Y.; Liang, J.; Zeng, G. M.; Wu, Z. B.; Wang, H. Doping of graphitic carbon nitride for photocatalysis: A reveiw. *Appl. Catal. B*: *Environ.* **2017**, *217*, 388–406.
[55] Zhu, B. C.; Zhang, L. Y.; Cheng, B.; Yu, J. G. First-principle calculation study of tri-s-triazine-based g-C_3N_4: A review. *Appl. Catal. B*: *Environ.* **2018**, *224*, 983–999.
[56] Mousavi, M.; Habibi-Yangjeh, A.; Pouran, S. R. Review on magnetically separable graphitic carbon nitride-based nanocomposites as promising visible-light-driven photocatalysts. *J. Mater. Sci.*: *Mater. Electron.* **2018**, *29*, 1719–1747.
[57] Baughman, R. H. Solid-state synthesis of large polymer single crystals. *J. Polym. Sci.*: *Polym. Phys. Ed.* **1974**, *12*, 1511–1535.
[58] Wang, W. H.; Zhan, Y. J.; Wang, G. H. One-step, solid-state reaction to the synthesis of copper oxide nanorods in the presence of a suitable surfactant. *Chem. Commun.* **2001**, *8*, 727–728.
[59] Ganesh, I.; Srinivas, B.; Johnson, R.; Saha, B. P.; Mahajan, Y. R. Microwave assisted solid state reaction synthesis of $MgAl_2O_4$ spinel powders. *J. Eur. Ceram. Soc.* **2004**, *24*, 201–207.
[60] Kouvetakis, J.; Todd, M.; Wilkens, B.; Bandari, A.; Cave, N. Novel synthetic routes to carbon-nitrogen thin films. *Chem. Mater.* **1994**, *6*, 811–814.
[61] Khabashesku, V. N.; Zimmerman, J. L.; Margrave, J. L. Powder synthesis and characterization of amorphous carbon nitride. *Chem. Mater.* **2000**, *12*, 3264–3270.
[62] Zhang, Z. H.; Leinenweber, K.; Bauer, M.; Garvie, L. A. J.; McMillan, P. F.; Wolf, G. H. High-pressure bulk synthesis of crystalline $C_6N_9H_3$·HCl: A novel C_3N_4 graphitic derivative. *J. Am. Chem. Soc.* **2001**, *123*, 7788–7796.
[63] Gu, Y. L.; Chen, L. Y.; Shi, L.; Ma, J. H.; Yang, Z. H.; Qian, Y. T. Synthesis of C_3N_4 and graphite by reacting cyanuric chloride with calcium cyanamide. *Carbon* **2003**, *41*, 2674–2676.
[64] Lu, X. F.; Gai, L. G.; Cui, D. L.; Wang, Q. L.; Zhao, X.; Tao, X. T. Synthesis and characterization of C_3N_4 nanowires and pseudocubic C_3N_4 polycrystalline nanoparticles. *Mater. Lett.* **2007**, *61*, 4255–4258.
[65] Shaikh, A. V.; Mane, R. S.; Joo, O. S.; Han, S. H.; Pathan, H. M. Electrochemical deposition of cadmium selenide films and their properties: A review. *J. Solid State Electrochem.* **2017**, *21*, 2517–2530.
[66] Li, J. D.; Zhang, X. L.; Raziq, F.; Wang, J. S.; Liu, C.; Liu, Y. D.; Sun, J. W.; Yan, R.; Qu, B. H.; Qin, C. L. et al. Improved photocatalytic activities of g-C_3N_4 nanosheets by effectively trapping holes with halogen-induced surface polarization and 2,4-dichlorophenol decomposition mechanism. *Appl. Catal. B*: *Environ.* **2017**, *218*, 60–67.
[67] Ozel, T.; Zhang, B. A.; Gao, R. X.; Day, R. W.; Lieber, C. M.; Nocera, D. G. Electrochemical deposition of conformal and functional layers on high aspect ratio silicon micro/nanowires. *Nano Lett.* **2017**, *17*, 4502–4507.
[68] Fu, Q.; Cao, C. B.; Zhu, H. S. Preparation of carbon nitride films with high nitrogen content by electrodeposition from an organic solution. *J. Mater. Sci. Lett.* **1999**, *18*, 1485–1488.
[69] Li, C.; Cao, C. B.; Zhu, H. S. Graphitic carbon nitride thin films deposited by electrodeposition. *Mater. Lett.* **2004**, *58*, 1903–1906.
[70] Bai, X. J.; Li, J.; Cao, C. B. Synthesis of hollow carbon nitride microspheres by an electrodeposition method. *Appl. Surf. Sci.* **2010**, *256*, 2327–2331.
[71] Chen, T.; Hao, Q.; Yang, W. J.; Xie, C. L.; Chen, D. M.; Ma, C.; Yao, W. Q.; Zhu, Y. F. A honeycomb multilevel structure Bi_2O_3 with highly efficient catalytic activity driven by bias voltage and oxygen defect. *Appl. Catal. B*: *Environ.* **2018**, *237*, 442–448.
[72] Ni, Z.; Masel, R. I. Rapid production of metal-organic frameworks via microwave-assisted solvothermal synthesis. *J. Am. Chem. Soc.* **2006**, *128*, 12394–12395.
[73] Yang, H. G.; Liu, G.; Qiao, S. Z.; Sun, C. H.; Jin, Y. G.; Smith, S. C.; Zou, J.; Cheng, H. M.; Lu, G. Q. Solvothermal synthesis and photoreactivity of anatase TiO_2 nanosheets with dominant {001} Facets. *J. Am. Chem. Soc.* **2009**, *131*, 4078–4083.
[74] Choucair, M.; Thordarson, P.; Stride, J. A. Gram-scale production of graphene based on solvothermal synthesis and sonication. *Nat. Nanotechnol.* **2009**, *4*, 30–33.
[75] Montigaud, H.; Tanguy, B.; Demazeau, G.; Alves, I.; Courjault, S. C_3N_4: Dream or reality? Solvothermal synthesis as macroscopic samples of the C_3N_4 graphitic form. *J. Mater. Sci.* **2000**, *35*, 2547–2552.
[76] Guo, Q. X.; Xie, Y.; Wang, X. J.; Lv, S. C.; Hou, T.; Liu, X. M. Characterization of well-crystallized graphitic carbon nitride nanocrystallites via a benzene-thermal route at low temperatures. *Chem. Phys. Lett.* **2003**, *380*, 84–87.
[77] Guo, Q. X.; Xie, Y.; Wang, X. J.; Zhang, S. Y.; Hou, T.; Lv, S. C. Synthesis of carbon nitride nanotubes with the C_3N_4 stoichiometry via a benzene-thermal process at low temperatures. *Chem. Commun.* **2004**, 26–27.
[78] Bai, Y. J.; Lü, B.; Liu, Z. G.; Li, L.; Cui, D. L.; Xu, X. G.; Wang, Q. L. Solvothermal preparation of graphite-like C_3N_4 nanocrystals. *J. Cryst. Growth* **2003**, *247*, 505–508.
[79] Li, J.; Cao, C. B.; Zhu, H. S. Synthesis and characterization of graphite-like carbon nitride nanobelts and nanotubes. *Nanotechnology* **2007**, *18*, 115605.
[80] Gillan, E. G. Synthesis of nitrogen-rich carbon nitride networks from an energetic molecular azide precursor. *Chem. Mater.* **2000**, *12*, 3906–3912.
[81] Lotsch, B. V.; Schnick, W. From triazines to heptazines: Novel nonmetal tricyanomelaminates as precursors for graphitic carbon nitride materials. *Chem. Mater.* **2006**, *18*, 1891–1900.
[82] Li, Y. Y.; Xue, L. H.; Fan, L. F.; Yan, Y. W. The effect of citric acid to metal nitrates molar ratio on sol–gel combustion synthesis of nanocrystalline $LaMnO_3$ powders. *J. Alloys Compd.* **2009**, *478*, 493–497.
[83] Dong, F.; Wu, L. W.; Sun, Y. J.; Fu, M.; Wu, Z. B.; Lee, S. C. Efficient synthesis of polymeric g-C_3N_4 layered materials as novel efficient visible light driven photocatalysts. *J. Mater. Chem.* **2011**, *21*, 15171–15174.
[84] Hong, J. H.; Xia, X. Y.; Wang, Y. S.; Xu, R. Mesoporous carbon nitride with *in situ* sulfur doping for enhanced photocatalytic hydrogen evolution from water under visible light. *J. Mater. Chem.* **2012**, *22*, 15006–15012.

[85] Cui, Y. J.; Ding, Z. X.; Liu, P.; Antonietti, M.; Fu, X. Z.; Wang, X. C. Metal-free activation of H_2O_2 by g-C_3N_4 under visible light irradiation for the degradation of organic pollutants. *Phys. Chem. Chem. Phys.* **2012**, *14*, 1455–1462.

[86] Dong, F.; Wang, Z. Y.; Sun, Y. J.; Ho, W. K.; Zhang, H. D. Engineering the nanoarchitecture and texture of polymeric carbon nitride semiconductor for enhanced visible light photocatalytic activity. *J. Colloid Interface Sci.* **2013**, *401*, 70–79.

[87] Long, B. H.; Lin, J. L.; Wang, X. C. Thermally-induced desulfurization and conversion of guanidine thiocyanate into graphitic carbon nitride catalysts for hydrogen photosynthesis. *J. Mater. Chem. A* **2014**, *2*, 2942–2951.

[88] Lan, Z. A.; Zhang, G. G.; Wang, X. C. A facile synthesis of Br-modified g-C_3N_4 semiconductors for photoredox water splitting. *Appl. Catal. B Environ.* **2016**, *192*, 116–125.

[89] Shan, W. J.; Hu, Y.; Bai, Z. G.; Zheng, M. M.; Wei, C. H. *In situ* preparation of g-C_3N_4/bismuth-based oxide nanocomposites with enhanced photocatalytic activity. *Appl. Catal. B: Environ.* **2016**, *188*, 1–12.

[90] Liu, S.; Tian, J. Q.; Wang, L.; Luo, Y. L.; Zhai, J. F.; Sun, X. P. Preparation of photoluminescent carbon nitride dots from CCl_4 and 1,2-ethylenediamine: A heat-treatment-based strategy. *J. Mater. Chem.* **2011**, *21*, 11726–11729.

[91] Liu, S.; Wang, L.; Tian, J. Q.; Zhai, J. F.; Luo, Y. L.; Lu, W. B.; Sun, X. P. Acid-driven, microwave-assisted production of photoluminescent carbon nitride dots from N,N-dimethylformamide. *RSC Adv.* **2011**, *1*, 951–953.

[92] Liu, S.; Tian, J. Q.; Wang, L.; Luo, Y. L.; Sun, X. P. A general strategy for the production of photoluminescent carbon nitride dots from organic amines and their application as novel peroxidase-like catalysts for colorimetric detection of H_2O_2 and glucose. *RSC Adv.* **2012**, *2*, 411–413.

[93] Barman, S.; Sadhukhan, M. Facile bulk production of highly blue fluorescent graphitic carbon nitride quantum dots and their application as highly selective and sensitive sensors for the detection of mercuric and iodide ions in aqueous media. *J. Mater. Chem.* **2012**, *22*, 21832–21837.

[94] Tang, Y. R.; Su, Y. Y.; Yang, N.; Zhang, L. C.; Lv, Y. Carbon nitride quantum dots: A novel chemiluminescence system for selective detection of free chlorine in water. *Anal. Chem.* **2014**, *86*, 4528–4535.

[95] Li, H.; Shao, F. Q.; Huang, H.; Feng, J. J.; Wang, A. J. Eco-friendly and rapid microwave synthesis of green fluorescent graphitic carbon nitride quantum dots for *vitro* bioimaging. *Sens. Actuators B: Chem.* **2016**, *226*, 506–511.

[96] Cao, X. T.; Ma, J.; Lin, Y. P.; Yao, B. X.; Li, F. M.; Weng, W.; Lin, X. C. A facile microwave-assisted fabrication of fluorescent carbon nitride quantum dots and their application in the detection of mercury ions. *Spectrochim. Acta A* **2015**, *151*, 875–880.

[97] Zhang, X. D.; Wang, H. X.; Wang, H.; Zhang, Q.; Xie, J. F.; Tian, Y. P.; Wang, J.; Xie, Y. Single-layered graphitic-C_3N_4 quantum dots for two-photon fluorescence imaging of cellular nucleus. *Adv. Mater.* **2014**, *26*, 4438–4443.

[98] Bai, X. J.; Yan, S. C.; Wang, J. J.; Wang, L.; Jiang, W. J.; Wu, S. L.; Sun, C. P.; Zhu, Y. F. A simple and efficient strategy for the synthesis of a chemically tailored g-C_3N_4 material. *J. Mater. Chem. A* **2014**, *2*, 17521–17529.

[99] Chen, X.; Liu, Q.; Wu, Q. L.; Du, P. W.; Zhu, J.; Dai, S. Y.; Yang, S. F. Incorporating graphitic carbon nitride (g-C_3N_4) quantum dots into bulk-heterojunction polymer solar cells leads to efficiency enhancement. *Adv. Funct. Mater.* **2016**, *26*, 1719–1728.

[100] Wang, X. P.; Wang, L. X.; Zhao, F.; Hu, C. G.; Zhao, Y.; Zhang, Z. P.; Chen, S. L.; Shi, G. Q.; Qu, L. T. Monoatomic-thick graphitic carbon nitride dots on graphene sheets as an efficient catalyst in the oxygen reduction reaction. *Nanoscale* **2015**, *7*, 3035–3042.

[101] Song, Z. P.; Lin, T. R.; Lin, L. H.; Lin, S.; Fu, F. F.; Wang, X. C.; Guo, L. Q. Invisible security ink based on water-soluble graphitic carbon nitride quantum dots. *Angew. Chem., Int. Ed.* **2016**, *55*, 2773–2777.

[102] Fan, X. Q.; Feng, Y.; Su, Y. Y.; Zhang, L. C.; Lv, Y. A green solid-phase method for preparation of carbon nitride quantum dots and their applications in chemiluminescent dopamine sensing. *RSC Adv.* **2015**, *5*, 55158–55164.

[103] Li, X. H.; Zhang, J. S.; Chen, X. F.; Fischer, A.; Thomas, A.; Antonietti, M.; Wang, X. C. Condensed graphitic carbon nitride nanorods by nanoconfinement: Promotion of crystallinity on photocatalytic conversion. *Chem. Mater.* **2011**, *23*, 4344–4348.

[104] Zhang, J. S.; Guo, F. S.; Wang, X. C. An optimized and general synthetic strategy for fabrication of polymeric carbon nitride nanoarchitectures. *Adv. Funct. Mater.* **2013**, *23*, 3008–3014.

[105] Liu, J.; Huang, J. H.; Zhou, H.; Antonietti, M. Uniform graphitic carbon nitride nanorod for efficient photocatalytic hydrogen evolution and sustained photoenzymatic catalysis. *ACS Appl. Mater. Interfaces* **2014**, *6*, 8434–8440.

[106] Bai, X. J.; Wang, L.; Zong, R. L.; Zhu, Y. F. Photocatalytic activity enhanced via g-C_3N_4 nanoplates to nanorods. *J. Phys. Chem. C* **2013**, *117*, 9952–9961.

[107] Xu, L.; Xia, J. X.; Wang, L. G.; Ji, H. Y.; Qian, J.; Xu, H.; Wang, K.; Li, H. M. Graphitic carbon nitride nanorods for photo-electrochemical sensing of trace copper(II) ions. *Eur. J. Inorg. Chem.* **2014**, *23*, 3665–3673.

[108] Hu, S. Z.; Ma, L.; Xie, Y.; Li, F. Y.; Fan, Z. P.; Wang, F.; Wang, Q.; Wang, Y. J.; Kang, X. X.; Wu, G. Hydrothermal synthesis of oxygen functionalized S-P codoped g-C_3N_4 nanorods with outstanding visible light activity under anoxic conditions. *Dalton Trans.* **2015**, *44*, 20889–20897.

[109] Tang, Y. Q.; Yuan, M.; Jiang, B. J.; Xiao, Y. T.; Fu, Y.; Chen, S.; Deng, Z. P.; Pan, Q. J.; Tian, C. G.; Fu, H. G. Inorganic acid-derived hydrogen-bonded organic frameworks to form nitrogen-rich carbon nitrides for photocatalytic hydrogen evolution. *J. Mater. Chem. A* **2017**, *5*, 21979–21985.

[110] Li, H. J.; Qian, D. J.; Chen, M. Templateless infrared heating process for fabricating carbon nitride nanorods with efficient photocatalytic H_2 evolution. *ACS Appl. Mater. Interfaces* **2015**, *7*, 25162–25170.

[111] Suenaga, K.; Johansson, M. P.; Hellgren, N.; Broitman, E.; Wallenberg, L. R.; Colliex, C.; Sundgren, J. E.; Hultman, L. Carbon nitride nanotubulite-densely-packed and well-aligned tubular nanostructures. *Chem. Phys. Lett.* **1999**, *300*, 695–700.

[112] Sung, S. L.; Tsai, S. H.; Tseng, C. H.; Chiang, F. K.; Liu, X. W.; Shih, H. C. Well-aligned carbon nitride nanotubes synthesized in anodic alumina by electron cyclotron resonance chemical vapor deposition. *Appl. Phys. Lett.* **1999**, *74*, 197–199.

[113] Tragl, S.; Gibson, K.; Glaser, J.; Duppel, V.; Simon, A.; Meyer, H. J. Template assisted formation of micro- and nanotubular carbon nitride materials. *Solid State Commun.* **2007**, *141*, 529–534.

[114] Bian, S. W.; Ma, Z.; Song, W. G. Preparation and characterization of carbon nitride nanotubes and their applications as catalyst supporter. *J. Phys. Chem. C* **2009**, *113*, 8668–8672.

[115] Li, Y. G.; Zhang, J.; Wang, Q. S.; Jin, Y. X.; Huang, D. H.; Cui, Q. L.; Zou, G. T. Nitrogen-rich carbon nitride hollow vessels: Synthesis, characterization, and their properties. *J. Phys. Chem. B* **2010**, *114*, 9429–9434.

[116] Cao, C. B.; Huang, F. L.; Cao, C. T.; Li, J.; Zhu, H. S. Synthesis of carbon nitride nanotubes via a catalytic-assembly solvothermal route. *Chem. Mater.* **2004**, *16*, 5213–5215.

[117] Jordan, T.; Fechler, N.; Xu, J. S.; Brenner, T. J. K.; Antonietti, M.; Shalom, M. "Caffeine doping" of carbon/nitrogen-based organic catalysts: Caffeine as a supramolecular edge modifier for the synthesis of photoactive carbon nitride tubes. *ChemCatChem* **2015**, *7*, 2826–2830.

[118] Guo, S. E.; Deng, Z. P.; Li, M. X.; Jiang, B. J.; Tian, C. G.; Pan, Q. J.; Fu, H. G. Phosphorus-doped carbon nitride tubes with a layered micro-nanostructure for enhanced visible-light photocatalytic hydrogen evolution. *Angew. Chem., Int. Ed.* **2016**, *55*, 1830–1834.

[119] Jin, Z. Y.; Zhang, Q. T.; Yuan, S. S.; Ohno, T. Synthesis high specific surface area nanotube g-C_3N_4 with two-step condensation treatment of melamine to enhance photocatalysis properties. *RSC Adv.* **2015**, *5*, 4026–4029.

[120] Tahir, M.; Cao, C. B.; Mahmood, N.;Butt, F. K.; Mahmood, A.; Idrees, F.;Hussain, S.; Tanveer, M.; Ali, Z.; Aslam, I. Multifunctional g-C_3N_4 nanofibers: A template-free fabrication and enhanced optical, electrochemical, and photocatalyst properties. *ACS Appl. Mater. Interfaces* **2014**, *6*, 1258–1265.

[121] Xie, M.; Wei, W.; Jiang, Z. F.; Xu, Y. G.; Xie, J. M. Carbon nitride nanowires/nanofibers: A novel template-free synthesis from a cyanuric

chloride-melamine precursor towards enhanced adsorption and visible-light photocatalytic performance. *Ceram. Int.* **2016**, *42*, 4158–4170.

[122] Han, Q.; Wang, B.; Zhao, Y.; Hu, C. G.; Qu, L. T. A graphitic-C_3N_4 "seaweed" architecture for enhanced hydrogen evolution. *Angew. Chem., Int. Ed.* **2015**, *54*, 11433–11437.

[123] Zhang, K.; Wang, L. Y.; Sheng, X. W.; Ma, M.; Jung, M. S.; Kim, W.; Lee, H.; Park, J. H. Tunable bandgap energy and promotion of H_2O_2 oxidation for overall water splitting from carbon nitride nanowire bundles. *Adv. Energy Mater.* **2016**, *6*, 1502352.

[124] Niu, P.; Zhang, L. L.; Liu, G.; Cheng, H. M. Graphene-like carbon nitride nanosheets for improved photocatalytic activities. *Adv. Funct. Mater.* **2012**, *22*, 4763–4770.

[125] Li, Y. F.; Jin, R. X.; Xing, Y.; Li, J. Q.; Song, S. Y.; Liu, X. C.; Li, M.; Jin, R. C. Macroscopic foam-like holey ultrathin g-C_3N_4 nanosheets for drastic improvement of visible-light photocatalytic activity. *Adv. Energy Mater.* **2016**, *6*, 1601273.

[126] Gholipour, M. R.; Béland, F.; Do, T. O. Post-calcined carbon nitride nanosheets as an efficient photocatalyst for hydrogen production under visible light irradiation. *ACS Sustainable Chem. Eng.* **2017**, *5*, 213–220.

[127] Zhang, X. D.; Xie, X.; Wang, H.; Zhang, J. J.; Pan, B. C.; Xie, Y. Enhanced photoresponsive ultrathin graphitic-phase C_3N_4 nanosheets for bioimaging. *J. Am. Chem. Soc.* **2013**, *135*, 18–21.

[128] Lu, Y. T.; Chu, D. M.; Zhu, M. S.; Du, Y. K.; Yang, P. Exfoliated carbon nitride nanosheets decorated with NiS as an efficient noble-metal-free visible-light-driven photocatalyst for hydrogen evolution. *Phys. Chem. Chem. Phys.* **2015**, *17*, 17355–17361.

[129] Wang, X.; Hong, M. Z.; Zhang, F. W.; Zhuang, Z. Y.; Yu, Y. Recyclable nanoscale zero valent iron doped g-C_3N_4/MoS_2 for efficient photocatalysis of RhB and Cr(VI) driven by visible light. *ACS Sustainable Chem. Eng.* **2016**, *4*, 4055–4063.

[130] Bao, N.; Hu, X. D.; Zhang, Q. Z.; Miao, X. H.; Jie, X. Y.; Zhou, S. Synthesis of porous carbon-doped g-C_3N_4 nanosheets with enhanced visible-light photocatalytic activity. *Appl. Surf. Sci.* **2017**, *403*, 682–690.

[131] Fang, L. J.; Li, Y. H.; Liu, P. F.; Wang, D. P.; Zeng, H. D.; Wang, X. L.; Yang, H. G. Facile fabrication of large-aspect-ratio g-C_3N_4 nanosheets for enhanced photocatalytic hydrogen evolution. *ACS Sustainable Chem. Eng.* **2017**, *5*, 2039–2043.

[132] Xu, J.; Zhang, L. W.; Shi, R.; Zhu, Y. F. Chemical exfoliation of graphitic carbon nitride for efficient heterogeneous photocatalysis. *J. Mater. Chem. A* **2013**, *1*, 14766–14772.

[133] Zhao, H. X.; Yu, H. T.; Quan, X.; Chen, S.; Zhao, H. M.; Wang, H. Atomic single layer graphitic-C_3N_4: Fabrication and its high photocatalytic performance under visible light irradiation. *RSC Adv.* **2014**, *4*, 624–628.

[134] Zhao, H. X.; Yu, H. T.; Quan, X.; Chen, S.; Zhang, Y. B.; Zhao, H. M.; Wang, H. Fabrication of atomic single layer graphitic-C_3N_4 and its high performance of photocatalytic disinfection under visible light irradiation. *Appl. Catal. B: Environ.* **2014**, *152–153*, 46–50.

[135] Dang, X. M.; Zhang, X. F.; Zhang, W. Q.; Dong, X. L.; Wang, G. W.; Ma, C.; Zhang, X. X.; Ma, H. C.; Xue, M. Ultra-thin C_3N_4 nanosheets for rapid charge transfer in the core-shell heterojunction of α-sulfur@C_3N_4 for superior metal-free photocatalysis under visible light. *RSC Adv.* **2015**, *5*, 15052–15058.

[136] Bojdys, M. J.; Müller, J. O.; Antonietti, M.; Thomas, A. Ionothermal synthesis of crystalline, condensed, graphitic carbon nitride. *Chem.—Eur. J.* **2008**, *14*, 8177–8182.

[137] Cheng, N. Y.; Jiang, P.; Liu, Q.; Tian, J. Q.; Asiri, A. M.; Sun, X. P. Graphitic carbon nitride nanosheets: One-step, high-yield synthesis and application for Cu^{2+} detection. *Analyst* **2014**, *139*, 5065–5068.

[138] Liu, G. G.; Wang, T.; Zhang, H. B.; Meng, X. G.; Hao, D.; Chang, K.; Li, P.; Kako, T.; Ye, J. H. Nature-inspired environmental "phosphorylation" boosts photocatalytic H_2 production over carbon nitride nanosheets under visible-light irradiation. *Angew. Chem., Int. Ed.* **2015**, *54*, 13561–13565.

[139] Lu, X. L.; Xu, K.; Chen, P. Z.; Jia, K. C.; Liu, S.; Wu, C. Z. Facile one step method realizing scalable production of g-C_3N_4 nanosheets and study of their photocatalytic H_2 evolution activity. *J. Mater. Chem. A* **2014**, *2*, 18924–18928.

[140] Dong, G. H.; Jacobs, D. L.; Zang, L.; Wang, C. Y. Carbon vacancy regulated photoreduction of NO to N_2 over ultrathin g-C_3N_4 nanosheets. *Appl. Catal. B: Environ.* **2017**, *218*, 515–524.

[141] Yin, Y.; Han, J. C.; Zhang, X. H.; Zhang, Y. M.; Zhou, J. G.; Muir, D.; Sutarto, R.; Zhang, Z. H.; Liu, S. W.; Song, B. Facile synthesis of few-layer-thick carbon nitride nanosheets by liquid ammonia-assisted lithiation method and their photocatalytic redox properties. *RSC Adv.* **2014**, *4*, 32690–32697.

[142] Yu, Y. Z.; Zhou, Q.; Wang, J. G. The ultra-rapid synthesis of 2D graphitic carbon nitride nanosheets via direct microwave heating for field emission. *Chem. Commun.* **2016**, *52*, 3396–3399.

[143] Davis, M. E. Ordered porous materials for emerging applications. *Nature* **2002**, *417*, 813–821.

[144] Dong, G. H.; Zhang, L. Z. Porous structure dependent photoreactivity of graphitic carbon nitride under visible light. *J. Mater. Chem.* **2012**, *22*, 1160–1166.

[145] Liang, Q. H.; Li, Z.; Yu, X. L.; Huang, Z. H.; Kang, F. Y.; Yang, Q. H. Macroscopic 3D porous graphitic carbon nitride monolith for enhanced photocatalytic hydrogen evolution. *Adv. Mater.* **2015**, *27*, 4634–4639.

[146] Wu, X. Y.; Li, S. M.; Wang, B.; Liu, J. H.; Yu, M. From biomass chitin to mesoporous nanosheets assembled loofa sponge-like N-doped carbon/g-C_3N_4 3D network architectures as ultralow-cost bifunctional oxygen catalysts. *Micropor. Mesopor. Mater.* **2017**, *240*, 216–226.

[147] Tian, N.; Zhang, Y. H.; Li, X. W.; Xiao, K.; Du, X.; Dong, F.; Waterhouse, G. I. N.; Zhang, T. R.; Huang, H. W. Precursor-reforming protocol to 3D mesoporous g-C_3N_4 established by ultrathin self-doped nanosheets for superior hydrogen evolution. *Nano Energy* **2017**, *38*, 72–81.

[148] Wang, Y. G.; Xia, Q. N.; Bai, X.; Ge, Z. G.; Yang, Q.; Yin, C. C.; Kang, S. F.; Dong, M. D.; Li, X. Carbothermal activation synthesis of 3D porous g-C_3N_4/carbon nanosheets composite with superior performance for CO_2 photoreduction. *Appl. Catal. B: Environ.* **2018**, *239*, 196–203.

[149] Zhou, Y. J.; Li, J. Z.; Liu, C. Y.; Huo, P. W.; Wang, H. Q. Construction of 3D porous g-C_3N_4/AgBr/rGO composite for excellent visible light photocatalytic activity. *Appl. Surf. Sci.* **2018**, *458*, 586–596.

[150] Chen, Z. F.; Lu, S. C.; Wu, Q. L.; He, F.; Zhao, N. Q.; He, C. N.; Shi, C. S. Salt-assisted synthesis of 3D open porous g-C_3N_4 decorated with cyano groups for photocatalytic hydrogen evolution. *Nanoscale* **2018**, *10*, 3008–3013.

[151] Sun, J. H.; Zhang, J. S.; Zhang, M. W.; Antonietti, M.; Fu, X. Z.; Wang, X. C. Bioinspired hollow semiconductor nanospheres as photosynthetic nanoparticles. *Nat. Commun.* **2012**, *3*, 1139.

[152] Zhang, S. B.; Li, M.; Qiu, W. J.; Wei, Y.; Zhang, G. F.; Han, J. Y.; Wang, H.; Liu, X. Super small polymeric carbon nitride nanospheres with core-shell structure for photocatalysis. *ChemistrySelect* **2017**, *2*, 10580–10585.

[153] Chen, J. H.; Shi, W. B.; Zhang, X. Y.; Arandiyan, H.; Li, D. F.; Li, J. H. Roles of Li^+ and Zr^{4+} Cations in the catalytic performances of $Co_{1-x}M_xCr_2O_4$ (M = Li, Zr; x = 0–0.2) for Methane Combustion. *Environ. Sci. Technol.* **2011**, *45*, 8491–8497.

[154] Cai, J. B.; Wu, X. Q.; Li, Y. H.; Lin, Y.; Yang, H.; Li, S. X. Noble metal sandwich-like TiO_2@Pt@C_3N_4 hollow spheres enhance photocatalytic performance. *J. Colloid Interface Sci.* **2018**, *514*, 791–800.

[155] Jun, Y. S.; Lee, E. Z.; Wang, X. C.; Hong, W. H.; Stucky, G. D.; Thomas, A. From melamine-cyanuric acid supramolecular aggregates to carbon nitride hollow spheres. *Adv. Funct. Mater.* **2013**, *23*, 3661–3667.

[156] Yang, J. J.; Chen, D. M.; Zhu, Y.; Zhang, Y. M.; Zhu, Y. F. 3D-3D porous Bi_2WO_6/graphene hydrogel composite with excellent synergistic effect of adsorption-enrichment and photocatalytic degradation. *Appl. Catal. B: Environ.* **2017**, *205*, 228–237.

[157] Tong, Z. W.; Yang, D.; Shi, J. F.; Nan, Y. H.; Sun, Y. Y.; Jiang, Z. Y. Three-dimensional porous aerogel constructed by g-C_3N_4 and graphene oxide nanosheets with excellent visible-light photocatalytic performance. *ACS Appl. Mater. Interfaces* **2015**, *7*, 25693–25701.

[158] Wang, X.; Liang, Y. H.; An, W. J.; Hu, J. S.; Zhu, Y. F.; Cui, W. Q. Removal of chromium (VI) by a self-regenerating and metal free g-C_3N_4/graphene hydrogel system via the synergy of adsorption and photo-catalysis under visible light. *Appl. Catal. B: Environ.*

2017, *219*, 53–62.
[159] Liang, Y. H.; Wang, X.; An, W. J.; Li, Y.; Hu, J. S.; Cui, W. Q. A g-C_3N_4@ppy-rGO 3D structure hydrogel for efficient photocatalysis. *Appl. Surf. Sci.* **2019**, *466*, 666–672.
[160] Zhang, M.; Luo, W. J.; Wei, Z.; Jiang, W. J.; Liu, D.; Zhu, Y. F. Separation free C_3N_4/SiO_2 hybrid hydrogels as high active photocatalysts for TOC removal. *Appl. Catal. B: Environ.* **2016**, *194*, 105–110.
[161] Zhang, M.; Jiang, W. J.; Liu, D.; Wang, J.; Liu, Y. F.; Zhu, Y. Y.; Zhu, Y. F. Photodegradation of phenol via C_3N_4-agar hybrid hydrogel 3D photocatalysts with free separation. *Appl. Catal. B: Environ.* **2016**, *183*, 263–268.
[162] Yan, J.; Rodrigues, M. T. F.; Song, Z. L.; Li, H. P.; Xu, H.; Liu, H.; Wu, J. J.; Xu, Y. G.; Song, Y. H.; Liu, Y. et al. Reversible formation of g-C_3N_4 3D hydrogels through ionic liquid activation: Gelation behavior and room-temperature gas-sensing properties. *Adv. Funct. Mater.* **2017**, *27*, 1700653.
[163] Zhang, Y. Y.; Zhou, Z. X.; Shen, Y. F.; Zhou, Q.; Wang, J. H.; Liu, A. R.; Liu, S. Q.; Zhang, Y. J. Reversible assembly of graphitic carbon nitride 3D network for highly selective dyes absorption and regeneration. *ACS Nano* **2016**, *10*, 9036–9043.
[164] Dong, F.; Zhao, Z.; Sun, Y.; Zhang, Y.; Yan, S.; Wu, Z. An advanced semimetal-organic Bi spheres-*g*-C_3N_4 nanohybrid with SPR-enhanced visible-light photocatalytic performance for NO purification. *Environ. Sci. Technol.* **2015**, *49*, 12432–12440.
[165] Xu, Y. L.; Niu, X. Y.; Zhang, H. J.; Xu, L. F.; Zhao, S. G.; Chen, H. L.; Chen, X. G. Switch-on fluorescence sensing of glutathione in food samples based on a graphitic carbon nitride quantum dot (g-CNQD)-Hg^{2+} chemosensor. *J. Agric. Food Chem.* **2015**, *63*, 1747–1755.
[166] Lin, X.; Xu, D.; Zheng, J.; Song, M. S.; Che, G. B.; Wang, Y. S.; Yang, Y.; Liu, C.; Zhao, L. N.; Chang, L. M. Graphitic carbon nitride quantum dots loaded on leaf-like $InVO_4/BiVO_4$ nanoheterostructures with enhanced visible-light photocatalytic activity. *J. Alloys Compd.* **2016**, *688*, 891–898.
[167] Yin, Y.; Zhang, Y. M.; Gao, T. L.; Yao, T.; Han, J. C.; Han, Z. B.; Zhang, Z. H.; Wu, Q.; Song, B. One-pot evaporation-condensation strategy for green synthesis of carbon nitride quantum dots: An efficient fluorescent probe for ion detection and bioimaging. *Mater. Chem. Phys.* **2017**, *194*, 293–301.
[168] Sun, B.; Lu, N.; Su, Y.; Yu, H. T.; Meng, X. Y.; Gao, Z. M. Decoration of TiO_2 nanotube arrays by graphitic-C_3N_4 quantum dots with improved photoelectrocatalytic performance. *Appl. Surf. Sci.* **2017**, *394*, 479–487.
[169] Su, J. Y.; Zhu, L.; Chen, G. H. Ultrasmall graphitic carbon nitride quantum dots decorated self-organized TiO_2 nanotube arrays with highly efficient photoelectrochemical activity. *Appl. Catal. B: Environ.* **2016**, *186*, 127–135.
[170] Zhang, H.; Guo, L. H.; Zhao, L. X.; Wan, B.; Yang, Y. Switching oxygen reduction pathway by exfoliating graphitic carbon nitride for enhanced photocatalytic phenol degradation. *J. Phys. Chem. Lett.* **2015**, *6*, 958–963.
[171] Chen, W.; Duan, G. R.; Liu, T. Y.; Chen, S. M.; Liu, X. H. Fabrication of Bi_2MoO_6 nanoplates hybridized with g-C_3N_4 nanosheets as highly efficient visible light responsive heterojunction photocatalysts for rhodamine B degradation. *Mater. Sci. Semicond. Process* **2015**, *35*, 45–54.
[172] Li, Y.; Liu, X. M.; Tan, L.; Cui, Z. D.; Yang, X. J.; Zheng, Y. F.; Yeung, K. W. K.; Chu, P. K.; Wu, S. L. Rapid sterilization and accelerated wound healing using Zn^{2+} and graphene oxide modified g-C_3N_4 under dual light irradiation. *Adv. Funct. Mater.* **2018**, *28*, 1800299.
[173] Fan, Y. D.; Zhou, J.; Zhang, J.; Lou, Y. Q.; Huang, Z. W.; Ye, Y.; Jia, L.; Tang, B. Photocatalysis and self-cleaning from g-C_3N_4 coated cotton fabrics under sunlight irradiation. *Chem. Phys. Lett.* **2018**, *699*, 146–154.
[174] Tian, J. Q.; Liu, Q.; Asiri, A. M.; Al-Youbi, A. O.; Sun, X. P. Ultrathin graphitic carbon nitride nanosheet: A highly efficient fluorosensor for rapid, ultrasensitive detection of Cu^{2+}. *Anal. Chem.* **2013**, *85*, 5595–5599.
[175] Shiravand, G.; Badiei, A.; Ziarani, G. M. Carboxyl-rich g-C_3N_4 nanoparticles: Synthesis, characterization and their application for selective fluorescence sensing of Hg^{2+} and Fe^{3+} in aqueous media. *Sens. Actuator B: Chem.* **2017**, *242*, 244–252.
[176] Wang, K.; Li, Q.; Liu, B. S.; Cheng, B.; Ho, W.; Yu, J. G. Sulfur-doped g-C_3N_4 with enhanced photocatalytic CO_2-reduction performance. *Appl. Catal. B: Environ.* **2015**, *176–177*, 44–52.
[177] Li, M.; Zhang, S. B.; Liu, X.; Han, J. Y.; Zhu, X. L.; Ge, Q. F.; Wang, H. Polydopamine and barbituric acid co-modified carbon nitride nanospheres for highly active and selective photocatalytic CO_2 reduction. *Eur. J. Inorg. Chem.* **2019**, *15*, 2058–2064.
[178] Zhang, Y. H.; Pan, Q. W.; Chai, G. Q.; Liang, M. R.; Dong, G. P.; Zhang, Q. Y.; Qiu, J. R. Synthesis and luminescence mechanism of multicolor-emitting g-C_3N_4 nanopowders by low temperature thermal condensation of melamine. *Sci. Rep.* **2013**, *3*, 1943.
[179] Das, D.; Shinde, S. L.; Nanda, K. K. Temperature-dependent photoluminescence of g-C_3N_4: Implication for temperature sensing. *ACS Appl. Mater. Interfaces* **2016**, *8*, 2181–2186.
[180] Chan, W. C. W.; Nie, S. M. Quantum dot bioconjugates for ultra-sensitive nonisotopic detection. *Science* **1998**, *281*, 2016–2018.
[181] Peng, M. S.; Wang, Y.; Fu, Q.; Sun, F. F.; Na, N.; Ouyang, J. Melanosome-targeting near-infrared fluorescent probe with large stokes shift for *in situ* quantification of tyrosinase activity and assessing drug effects on differently invasive melanoma cells. *Anal. Chem.* **2018**, *90*, 6206–6213.
[182] Cui, Q. L.; Xu, J. S.; Wang, X. Y.; Li, L. D.; Antonietti, M.; Shalom, M. Phenyl-modified carbon nitride quantum dots with distinct photoluminescence behavior. *Angew. Chem., Int. Ed.* **2016**, *55*, 3672–3676.
[183] Su, J. Y.; Zhu, L.; Geng, P.; Chen, G. H. Self-assembly graphitic carbon nitride quantum dots anchored on TiO_2 nanotube arrays: An efficient heterojunction for pollutants degradation under solar light. *J. Hazard. Mater.* **2016**, *316*, 159–168.
[184] Sun, S. M.; An, Q.; Wang, W. Z.; Zhang, L.; Liu, J. J.; Goddard III, W. A. Efficient photocatalytic reduction of dinitrogen to ammonia on bismuth monoxide quantum dots. *J. Mater. Chem. A* **2017**, *5*, 201–209.